AN EXPERIMENTAL METHOD TO INCREASE SEDIMENT SUPPLY TO A SALT MARSH IN SUBSIDENCE DOMINATED ENVIRONMENTS

A Thesis

by

ROBERT C. THOMAS

Submitted to the Office of Graduate Studies of
Texas A&M University
in partial fulfillment of the requirements for the degree of

MASTER OF SCIENCE

May 2007

Major Subject: Ocean Engineering

AN EXPERIMENTAL METHOD TO INCREASE SEDIMENT SUPPLY TO A SALT MARSH IN SUBSIDENCE DOMINATED ENVIRONMENTS

A Thesis

by

ROBERT C. THOMAS

Submitted to the Office of Graduate Studies of
Texas A&M University
in partial fulfillment of the requirements for the degree of

MASTER OF SCIENCE

Approved by:

Co-Chairs of Committee,	Tom Ravens
	Billy L. Edge
Committee Member,	Achim Stössel
Head of Department,	Tony Cahill

May 2007

Major Subject: Ocean Engineering

ABSTRACT

An Experimental Method to Increase Sediment Supply to
a Salt Marsh in Subsidence Dominated Environments. (May 2007)
Robert C. Thomas, B.S., Texas A&M University Galveston
Co-Chairs of Advisory Committee: Dr. Tom Ravens
Dr. Billy L. Edge

This thesis examines the environmental conditions which led to the loss of 90% of the natural salt marsh in Galveston Island State Park since 1930 and analyzes one potential method to reduce future loss. Available data and recent studies suggest that the primary factor responsible for the historic loss was the lack of a sufficient supply of sediment to keep up with relative sea level rise. The average rate of sediment accretion for the period from 1963 to 2006 was measured to be 0.25 cm/year based on ^{137}Cs and $^{239,240}Pu$ nuclides. This rate is about 0.4 cm/year less than the relative sea level rise of approximately 0.65 cm/year during the same period. The marsh restoration project, constructed in 1999 at the Galveston Island State Park, focused on reduction of wave induced erosion and direct replacement of marsh substrate through terracing. The restoration project did not address the potential for marsh lost to submergence.

As an alternative to geotubes or more permanent breakwater methods, a submerged sacrificial berm constructed around the marsh is a possible approach to address ongoing submergence. The sacrificial berm increases the available sediment supply by allowing partial transmission of waves to create a net transport of sediment into the marsh. In addition, the berm is designed to limit wave height in the marsh to reduce wave induced erosion. The proposed method involves iteratively adjusting the width and elevation of the berm top to maximize sediment transport from the berm into the marsh. A sediment transport model is developed to quantify the increased transport into the marsh, estimate a nourishment interval and qualitatively judge the expected berm evolution. The Galveston Island State Park marsh was used for demonstration

purposes; however, the restoration concept and method of analysis is applicable to other marshes in Galveston Bay.

TABLE OF CONTENTS

Page

ABSTRACT iii

TABLE OF CONTENTS v

LIST OF FIGURES vii

LIST OF TABLES viii

1. INTRODUCTION 1

1.1 Objectives 3
1.1.1 Environmental Conditions 3
1.1.2 Circulation Models 3
1.1.3 Factors Controlling Marsh Loss 3
1.1.4 Initial Impact of Waves and Currents on Sediment Transport 4
1.1.5 Wave Transformation and Berm Design 4
1.1.6 Sediment Transport Modeling 4

2. ENVIRONMENTAL CONDITIONS AT THE PROJECT SITE 6

2.1 Wind Conditions 6
2.2 Wave Conditions 7
2.3 Water Level Conditions 9
2.4 Relative Sea Level Rise 11
2.5 Sediment Accretion Rate 12

3. CIRCULATION MODEL OF GALVESTON BAY 14

4. CIRCULATION MODEL OF THE MARSH 15

5. FACTORS CONTROLLING MARSH LOSS 17

6. WAVE AND CURRENT IMPACT ON SEDIMENT TRANSPORT 19

7. BERM DESIGN 21

7.1 Wave Transformation Over The Berm 21
7.2 Berm Design Characteristics 23

8. HYDRODYNAMIC MODEL INCLUDING THE BERM 25

Page

9. SEDIMENT TRANSPORT MODELING 28
9.1 Non-Breaking Wave Transport 28
9.1.1 Suspended Load Concentration Profile 29
9.1.2 Laboratory Test to Calibrate Suspended Concentration 33
9.1.3 Velocity Profile 37
9.1.4 Suspended Load Transport Calculation 39
9.1.5 Bed Load 40
9.2 Breaking Wave Transport 41
9.2.1 Velocity Profile 41
9.2.2 Suspended Load Concentration Profile 43
9.2.3 Breaking Wave Transport Calculations 44
9.3 Net Transport Calculation Method 46
9.3.1 Comparison of Wave-Only Net Cross Shore Transport 47
10. SEDIMENT TRANSPORT RESULTS 49
11. CONCLUSION 54
REFERENCES 56
VITA 59

LIST OF FIGURES

Page

Figure 1: Galveston Island State Park - 2004 2
Figure 2: Wind Rose for 1997-2005 7
Figure 3: Example SWAN output. 8
Figure 4: Mean water level per wind direction. 11
Figure 5: RMA2 model verification. 16
Figure 6: RMA2 model velocity near entrance 2. 16
Figure 7: Simplified cross section of the berm. 26
Figure 8: Water velocity and elevation when the wind is from 300º. 27
Figure 9: Wave flume. 33
Figure 10: Grain size distribution of bed sediments. 35
Figure 11: Suspended grain size distributions as a function of maximum near bottom velocity. 35
Figure 12: Comparison of modeled vs. measured suspended concentration. 36
Figure 13: Comparison between measured and calculated velocity in the wave flume. 38
Figure 14: Cross shore transport with and without empirical breaking. 45
Figure 15: Cross-shore transport caused by waves only. 47
Figure 16: Cross shore variation of yearly net transport rate. 49
Figure 17: Cross-shore variation in the horizontal derivative of transport rate. 51
Figure 18: Net berm evolution after one year. 52

LIST OF TABLES

Page

Table 1: Wave height in meters at the edge of the marsh. 9
Table 2: 20% exceedence wave height per berm top elevation. 24
Table 3: Composition of Bay Sediments.....39
Table 4: Increase in transport due to modified velocity as a function of current.....45

1. INTRODUCTION

Wetlands in Galveston Bay are being lost at an alarming rate. Factors responsible include relative sea level rise, wave induced erosion, lack of sufficient sediment supply to keep pace with relative sea level rise, conversion to upland urban areas and other factors (White et al.. 1993). Photographic analysis of the period between 1950 and 1989 indicates at least a 17% net loss of wetlands in the Galveston Bay system with local net gains and extreme losses throughout the Bay (White et al. 1993).

Marsh restoration projects in Galveston Bay tend to involve the placement of geotube breakwaters to limit the potential wave induced erosion. An extensive network of geotube breakwaters was placed around the Galveston Island State Park marsh to prevent such erosion. The geotubes adequately reduce wave energy reaching the marsh but do not address the lack of sediment supply to keep pace with relative sea level rise. A potential alternative to the geotubes which might increase the sediment supply is a submerged sacrificial berm made of native sediment.

Galveston Island State Park marsh (Figure 1) lost 405 of its original 445 hectare area between 1930 and 1994 (Glass and Hollingsworth 1999). HDR Shiner Moseley and Associates was contracted in 1999 to build geotubes around the remnants of the marsh and construct approximately 80 hectares of earthen terrace marsh complex (HDR Shiner Moseley and Associates, Inc). Aerial photographs from 1930 were analyzed by The University of Texas, Bureau of Economic Geology to determine the historic shoreline. The 1930 shoreline is overlaid on the 2004 photograph shown in Figure 1.

This thesis follows the style of Coastal Engineering.

Following project completion, sea grass (*Halophila engelmanni* and *Halodule wrightii*) was observed over much of the Bay bottom inside the geotube protected area. The sea grass does not grow in the Bay outside the geotube protected marsh complex. The sea grass habitat is just as important and endangered as the salt marsh and the proposed project may adversely affect some of this habitat. The extent to which the sea grass might be further jeopardized is not quantified but it is noted that the continued subsidence in the area causes just as serious a problem for the sea grass as the salt marsh.

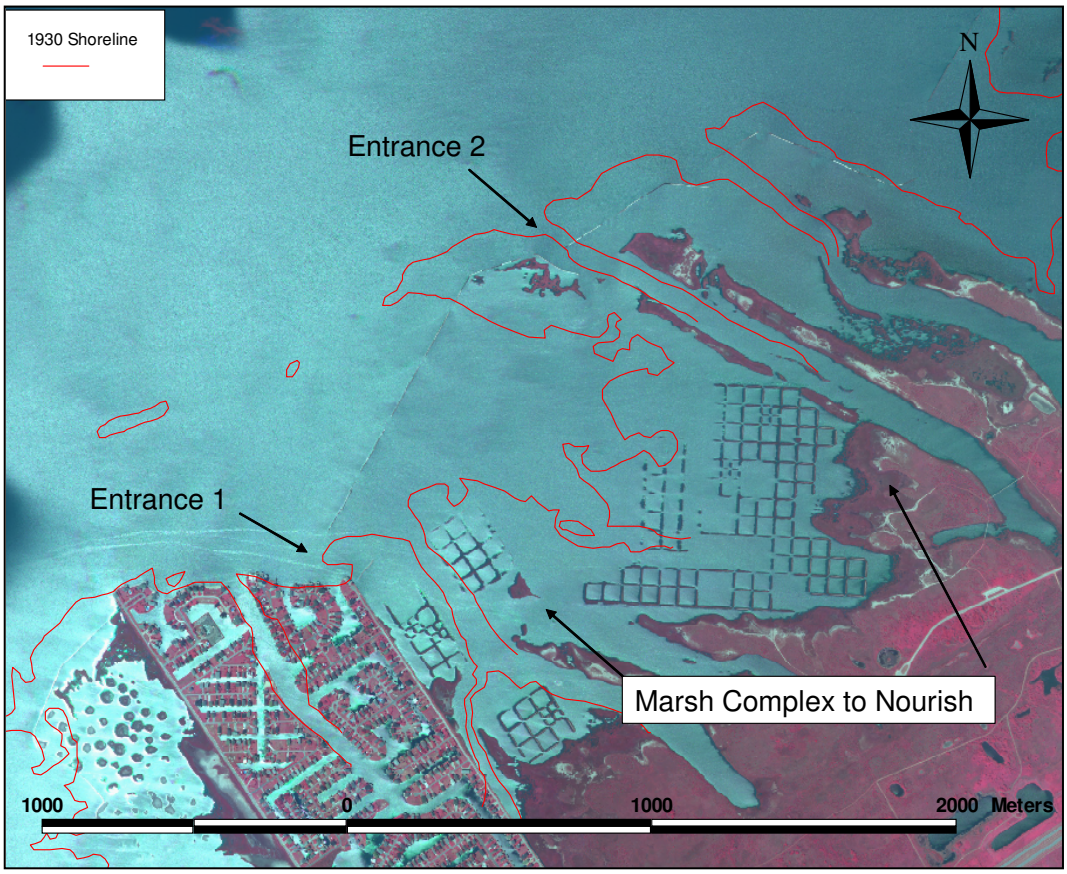

Figure 1: Galveston Island State Park - 2004

1.1 Objectives

The approach to solving the problem is outlined in the following sub-sections. When complete, the major factor controlling marsh loss in the State Park will be proven to be a lack of sediment supply to keep pace with relative sea level rise. A solution to prevent such loss is proposed and analyzed.

1.1.1 Environmental Conditions

Section 2 defines the environmental conditions at the marsh. Wave and water level conditions are determined for Galveston Bay near the State Park based on the statistical distribution of the winds. The relative sea level rise is defined as 0.65 cm/year. The rate of sediment accretion is measured to be considerably less, 0.25 cm/year.

1.1.2 Circulation Models

Circulation models are described and verified in sections 3 and 4. An ADCIRC model of Galveston Bay was developed to study water level and tidal circulation in the Bay near the State Park. RMA2 was used to model circulation in the marsh and was verified with velocity data collected near entrance 2 (Figure 1). The marsh circulation model provides currents to the sediment transport model.

1.1.3 Factors Controlling Marsh Loss

The factor controlling marsh loss is determined in Section 5. The large discrepancy between relative sea level rise and the rate of sediment accretion in the

marsh indicates that significant loss of salt marsh will occur. The wave conditions in the marsh are compared with published literature and an empirical equation developed for use on the East Coast. Both suggest that the wave induced erosion is of limited concern. No other factors influence marsh loss at the State Park.

1.1.4 Initial Impact of Waves and Currents on Sediment Transport

A submerged berm is proposed to protect the marsh from the limited wave action and to act as a source of sediment. Only the section of marsh behind the geotubes between entrances 1 and 2 is considered for this test case. Limiting the scope of the problem helps simplify some of the following work. Section 6 makes comparisons of the Shields parameters due to waves and currents separately. Comparison of the Shields parameters indicates that sediment suspension can be initiated with waves but not by the currents alone.

1.1.5 Wave Transformation and Berm Design

Section 7 describes the wave transformation model and uses the model to determine the wave conditions in the marsh as a function of berm design. The optimum berm design maximizes wave height in the marsh complex without allowing wave induced erosion. The circulation model of the marsh is modified to include the berm in Section 8.

1.1.6 Sediment Transport Modeling

Section 9 presents a method to calculate sediment transport over the berm including the effects of nonlinear waves. Transport is calculated in two modes,

suspended and bed load. A second order Stokes approximation is used to determine the wave velocity profile in the presence of currents. Wave breaking is solved in the same manner as the non-wave breaking case with an empirical amplification. The results are presented in Section 10. The yearly net transport is calculated to be approximately 1 m^3/year/m of berm width into the marsh. This rate is enough to double sediment supply to the marsh using the maximum available berm width, but still is not enough to keep pace with relative sea level rise.

2. ENVIRONMENTAL CONDITIONS AT THE PROJECT SITE

2.1 Wind Conditions

The wind data collected at the Galveston Pleasure Pier between 1997 and 2005 was used to determine the statistical distribution of the winds. The orientation of the marsh is such that only winds from between 195º and 045º degrees true need to be considered for wave induced erosion, all other directions will result in waves going away from the marsh which will not contribute to erosion. The distribution of wind speed per direction is shown in Figure 2. The axis units are the percent occurrence with the total percent occurrence from each direction subdivided to show the percentage per wind speed. The axes also represent the cardinal direction, North is up.

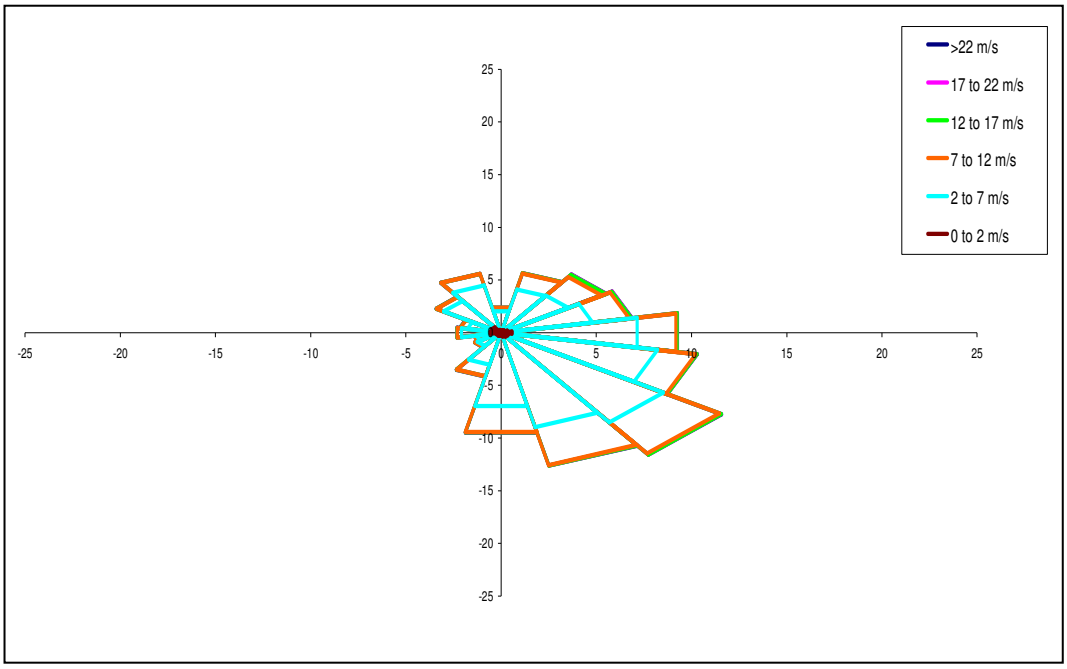

Figure 2: Wind Rose for 1997-2005

2.2 Wave Conditions

Texas A&M at Galveston developed a SWAN model for Galveston Bay that was used to calculate the wave conditions in the Bay for each wind condition (SWAN User Manual – TAMUG website). An example of the SWAN output in quasi-steady mode is shown in Figure 3. A comparison between the SWAN model and measurements made on 27 June 2006 proved that the model accurately predicts wave conditions near the marsh. The statistical distribution of the winds was used to determine the distribution of the waves in the Bay.

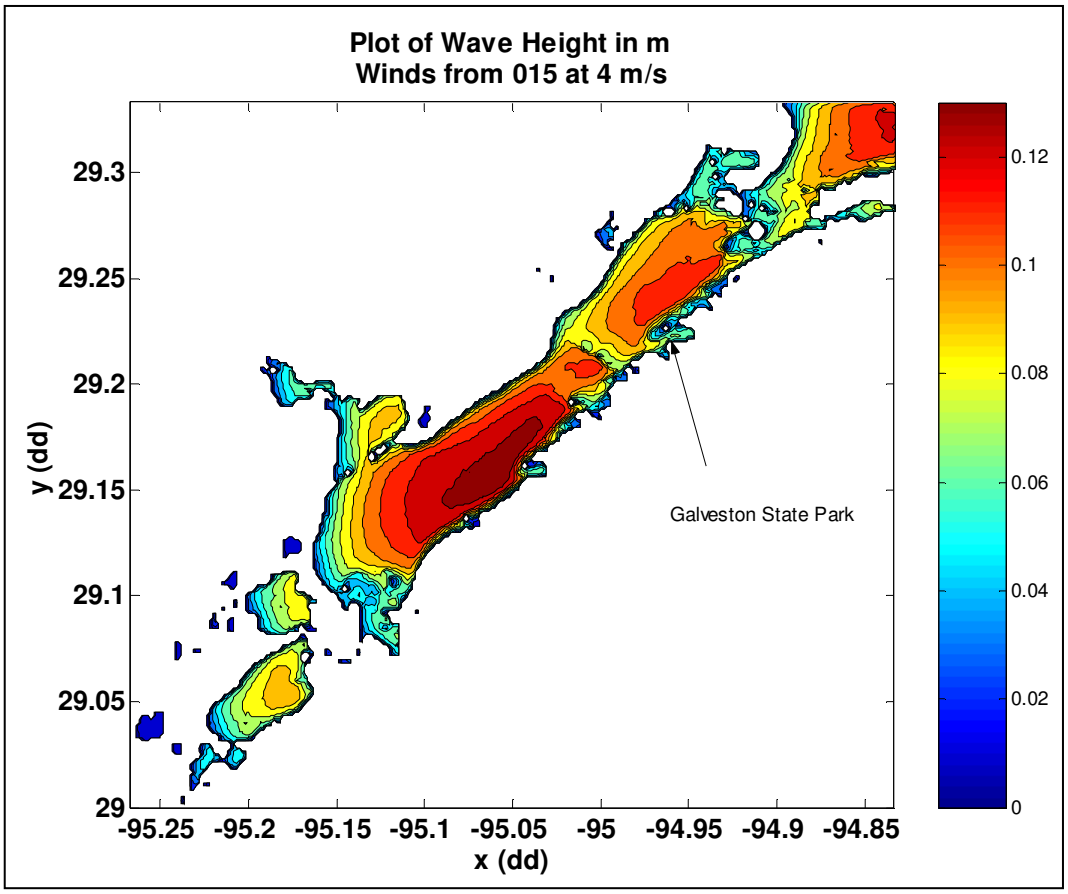

Figure 3: Example SWAN output.

Shafer, Roland, and Douglass (2003) made observations in Galveston Bay in order to determine the sustainability of marshes in different wave climates. They used a wave model depth averaged over the entire fetch, assuming that the fetch is zero for winds from the landward direction. The results of that analysis indicate that significant wave induced erosion will not occur when the 20% exceedence wave height is less than 0.14 m. Since SWAN is being used in this application and is a two-dimensional model, a location near the marsh with a depth comparable to the depth average is chosen. This location allows for waves generated from all directions. A location to the northwest of

entrance 1 with a water depth of 1.2 m relative to mean sea level (MSL) is chosen for wave analysis. The data is then analyzed to determine the 20% exceedence wave characteristics. Wave height during each wind condition is reported in Table 1.

Table 1: Wave height in meters at the edge of the marsh.

Winds from →	**0**	**30**	**210**	**240**	**270**	**300**	**330**
Wind Speed 2 m/s	0.05	0.05	0.05	0.05	0.05	0.05	0.05
Wind Speed 7 m/s	0.19	0.18	0.16	0.18	0.19	0.2	0.19
Wind Speed 12 m/s	0.3	0.27	0.25	0.27	0.3	0.31	0.3
Wind Speed 17 m/s	0.37	0.35	0.33	0.35	0.37	0.38	0.38
Wind Speed 22 m/s	0.42	0.41	0.38	0.4	0.41	0.42	0.43

The wave height in the marsh was calculated assuming the geotubes had not been constructed. Winds in each of the twelve, thirty degree, directional bins and for a range of wind speeds were used to find the wave height. Winds from 045 to 195 cause waves going away from the marsh, so they are not reported. Analysis of waves generated in all directions that could enter the marsh indicates a 20% exceedence wave height of 0.18 m, which is only slightly above the 0.14 m design condition. Wind directions that result in a wave direction going away from the marsh are considered to have a wave height at the marsh of H = 0.0 m.

2.3 Water Level Conditions

A relationship between water level and wave conditions must be developed in order to optimize the berm design. Winds from the north/northwest typically cause

extreme low water levels in Galveston Bay and occur during the winter months. Observations of water level were made with the calibrated Bay-scale ADCIRC model of water level at Pier 21 in Galveston and in the State Park. The model indicates that the tidal range near the State Park is within 80% of that at Pier 21. It will be assumed that the water level at Pier 21 can be substituted for a detailed analysis at the State Park, realizing that there will be some error induced.

The water level data is sorted into 40, five centimeter wide water level bins in order to determine the percent occurrence of each water level. That data is then used to calculate the mean water level for each wind direction. The mean water level of the total data set is the mean sea level (MSL) at Pier 21, 17.5 cm above mean low water (MLW). The calculated MSL is 1.5 cm higher than as calculated by the National Oceanic and Atmospheric Administration (NOAA) (2006). The discrepancy is probably due to the 8 year data set used here because of the limited wind data, as opposed to the 18 year (1983 – 2001) data set NOAA uses.

The dependence of mean water level on wind direction was also examined (Figure 4). The data shows that when the wind is from the west-northwest the water level is considerably lower, but when the wind blows directly from the north the water level is only slightly below average. The percent occurrence of each water level per wind direction will be used as an input to the wave transformation model in determining the average transmitted wave height.

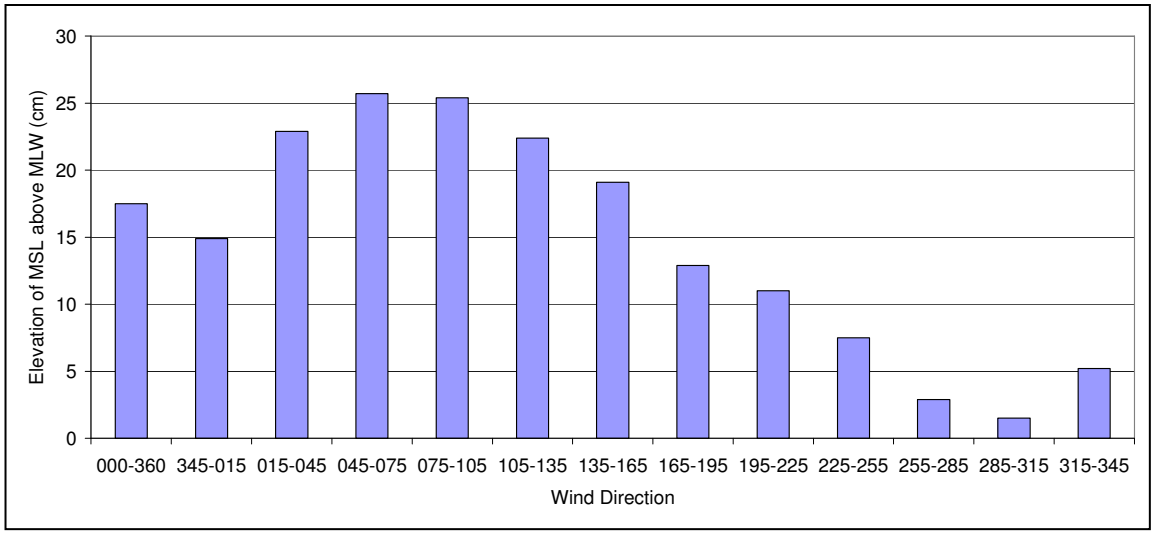

Figure 4: Mean water level per wind direction.

2.4 Relative Sea Level Rise

NOAA (2006) calculates relative sea level trends at its long term water level stations. The station nearest the area of interest is Pier 21 in Galveston. Relative sea level trends at Pier 21 are calculated based on the monthly mean sea level from 1908 to 1999 and indicate a mean increase of 0.65 cm per year (NOAA (2006)). The relative sea level rise is a measure of the absolute sea level rise and local subsidence. The Galveston Island State Park marsh is 22.5 km from Pier 21.

The study area and Pier 21 tide gauge are within the limits of area 1 of the Harris-Galveston Coastal Subsidence District (Harris Galveston Subsidence District). The District analyzed available data from 1906 – 1987 reporting a total net subsidence near Pier 21 of 30.5 cm (0.38 cm/year) with the same net subsidence reported in the State Park (Zilkoski et al. (2006)).

The closest operational subsidence measuring stations to the study area is Port-A-Measure (PAM) 26. PAM 26 is located at 29.21N 94.94W, 1.6 km from the State Park. It recorded a cumulative subsidence of approximately 1.22 cm over the period from 2002 to 2005. This is an average of 0.31 cm per year, which is slightly less than the long term average. The new data set suggests that a reasonable and conservative approach is to use the long term average, 0.65 cm per year, as the expected future rate of relative sea level rise.

2.5 Sediment Accretion Rate

Historic accretion rates in Galveston Bay have been calculated based on ^{137}Cs and $^{239,240}Pu$ nuclides which reached a maximum concentration in 1963 (Santschi et al.. 2001). The rate of accretion in Galveston Bay was collected in Trinity Bay at a rate of 0.38 cm/year (Santschi et al. 2001). Since the rate of accretion will indicate if there is a sufficient supply of sediment to sustain the marsh, this rate must be accurately quantified. Dr. Santschi was commissioned to analyze new cores in the marsh complex to determine the rate of sedimentation. The first core was collected at a location just below the mean high water line (MHW) and landward of any open water. The analysis of the first core indicates that the rate of accretion in the marsh is 0.25 (± 0.03) cm/year. A second core was collected in the same area of the marsh at the edge of the open water. The analysis of the second core indicates that the rate of accretion in the marsh is 0.25 $(+0.09, -0.07)$ cm/year.

The measured rates at both locations are insufficient to keep pace with relative sea level rise. This data suggests that the current sediment supply must be more than doubled for the marsh to avoid submergence. Proosdij et al. (2006) studied sediment accretion rate in the Bay of Fundy. They found that it can vary in a salt marsh with the highest deposition rates near MHW. While the tides in Galveston Bay are insignificant compared to those in the Bay of Fundy, the same trend will likely be found leading to

lower accretion rates in the large open water areas of the marsh complex. Lower accretion rates in the open water areas will result in an increased rate at which sea grass habitat is lost. Based on these initial measurements the sediment supply will need to be increased by at least a factor of two.

3. CIRCULATION MODEL OF GALVESTON BAY

An ADCIRC model of Galveston Bay was created for this study to investigate effects of wind and tides on the water level near the State Park. It also provides the boundary conditions for modeling circulation in the marsh. The model is forced with measured water surface elevations at San Luis Pass, the Galveston Entrance Channel, Rollover Pass and Morgans Point. An averaged wind and pressure field is applied over the entire domain. The use of an averaged wind induces some local error.

Rigorous verification using water level at Pier 21, Eagle Point and the Elm Grove marsh have a root mean square (RMS) error of less than 3.5 cm during the calibration period in October 2004. The solution is dependent on the variability in the wind fields; therefore, the accuracy of this model is dependent on having uniform wind across the Bay. Analysis during other periods has shown RMS error as high as 5.5 cm over a two week investigation. The typical spring neap tidal cycle near the Galveston Island State Park was determined based on the output of this model. The tidal range varies from 20 cm to 50 cm.

4. CIRCULATION MODEL OF THE MARSH

A circulation model of the Galveston Island State Park marsh complex was completed to investigate currents in the existing configuration and to provide currents to the sediment transport model. RMA2 is used to calculate water velocity and surface elevation in the marsh by solving the Reynolds form of the Navier-Stokes equations for turbulent flows in two horizontal dimensions (Donnell et al. 2005).

RMA2 is forced on the open boundaries with water surface elevations output from the large scale ADCIRC model and wind at each node. Comparison of the results including dynamic wind and without wind showed little variation. This coupled with the known issue of exaggerated set-up when a steady wind is applied (Donnell et al. 2005) prompted the decision to remove the wind from the calculations. The RMA2 model is calibrated by adjusting bottom roughness in the domain to match model velocity with data collected on two trips to the site. Roughness values of 0.25 were used in the model domain except in the regions of the marsh terraces where the roughness was 0.04. Radiation stress is not included.

The bathymetry in the vicinity of the marsh terraces is averaged in order to reduce the computational time of the problem. The reduction in resolution is done to reduce the required run time of the model. Detailed information about sediment exchange in the grass isn't required to estimate the supply of sediment to the marsh, making this simplification possible. The marsh affects on hydrodynamics are captured using increased roughness.

Figure 5 shows the velocity from the model of the existing configuration compared with the measured velocity. The data was collected 140 m inside the marsh complex at entrance 2. The comparison shows reasonable agreement with the measured data. The magnitude during a 19 day run at the same location for the existing condition is shown in Figure 6.

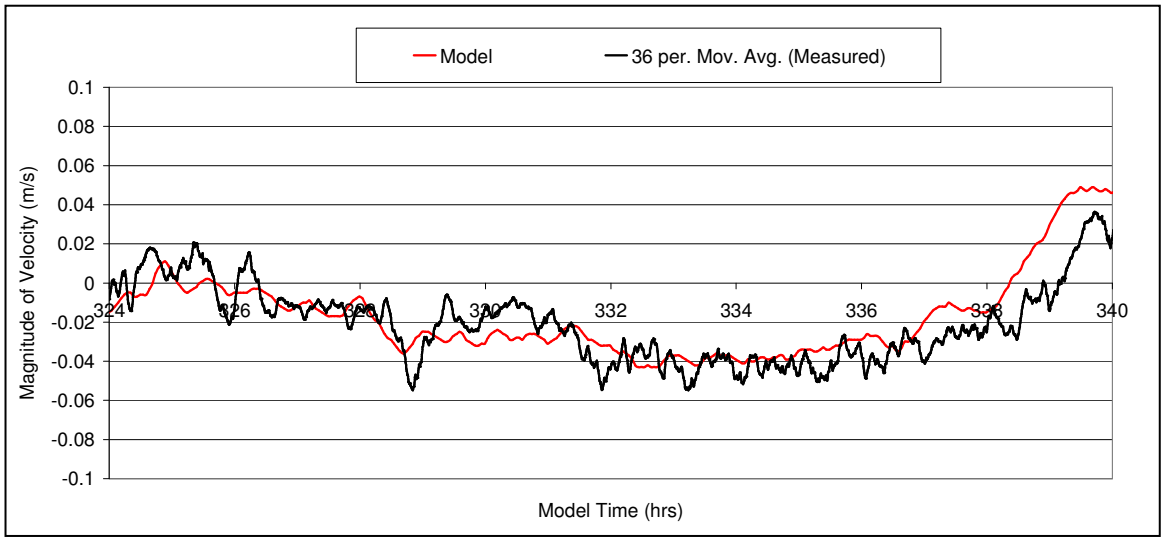

Figure 5: RMA2 model verification.

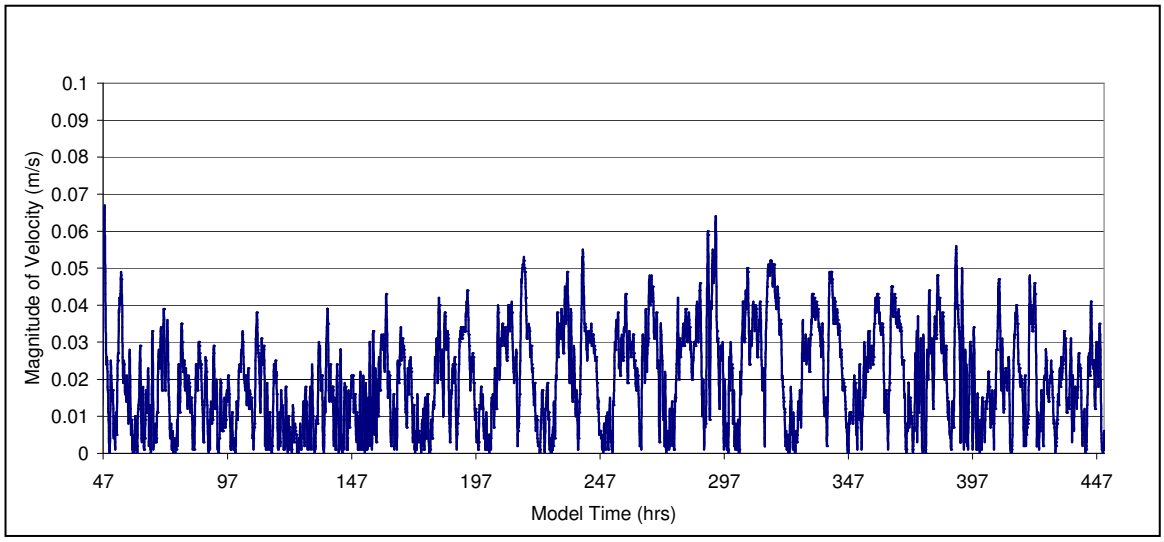

Figure 6: RMA2 model velocity near entrance 2.

5. FACTORS CONTROLLING MARSH LOSS

The two most likely potential sources of marsh loss at the Galveston Island State Park are wave-induced erosion and submergence. The measured sediment accretion rate and relative sea level rise show that significant loss will be caused by submergence. Shafer, Roland, and Douglass (2003) analyzed sites in Galveston Bay to determine the allowable wave heights that will cause erosion. Their results indicate that stable marshes should exist when the 20^{th} percentile exceedence wave height is less than 0.14 m. They also report that marshes with a 20^{th} percentile exceedence wave height greater than 0.3 m did not support extensive marsh vegetation.

Analysis of waves near Galveston Island State Park shows a 20^{th} percentile exceedence wave height of 0.18 m in the marsh if there were no geotubes. This indicates that the wave induced erosion in the marsh is probably of secondary concern to relative sea level rise. The original project documents (Shiner Moseley and Associates 1998) also recognize the importance of relative sea level rise but they don't rule out the potential for wave induced erosion.

Schwimmer (2001) made observations in Rehoboth Bay, Delaware, in an effort to relate wave power to erosion rate. An empirical equation (Equation 1) is presented in his work and will be applied here as an indicator of potential shoreline erosion.

$$R = 0.35P^{1.1} \qquad \textbf{(1)}$$

where R is the erosion rate in m/year, P = E*Cg is the wave power in (KW/m), E is the wave energy and Cg is the group velocity.

This equation can be used as an indicator of possible erosion. The wave analysis used in Schwimmer (2001) is similar to the one presented here and the 20^{th} percentile exceedence wave height will be used to determine the 20^{th} percentile exceedence erosion rate. Shallow water assumptions were used to estimate the wave power for the 20th percentile wave conditions of (H_{20} = 0.18 m, T_{20} = 1.7s, L_{20} = 4.26m) which gives an

erosion rate of 1.1 cm/year. The erosion rate calculated is low enough that it can be considered insignificant. Schwimmer's (2001) approach further proves that the primary cause of marsh loss at the State Park is relative sea level rise and a lack of sediment supply.

6. WAVE AND CURRENT IMPACT ON SEDIMENT TRANSPORT

An estimate of the maximum required sediment supply to the marsh can be calculated by multiplying the area of marsh by the relative sea level rise. This method indicates 8000 m^3/year is required to keep up with relative sea level rise for the entire marsh complex. This analysis is limited to nourish the section of the marsh behind entrances 1 and 2 in order to simplify the scope of the problem. That area of the marsh complex is approximately 500,000 m^2 which will require about 3250 m^3 /year to keep pace with relative sea level rise. The measured accretion rate of 0.25 cm/year is equivalent to about 1250 m^3 /year.

Hydrodynamic modeling in the marsh indicates that the maximum velocity over a typical spring-neap tidal cycle just a short distance from an entrance is about 5 cm/s. A comparison of the maximum instantaneous Shields parameter (ψ) with the critical value of the Shields parameter (ψ_{cr}) will indicate if sediment motion will occur (Madsen and Wood (2002)).

$$\psi = \frac{u_*^2}{(S-1)gD} \qquad \textbf{(2)}$$

where u_* is the shear velocity determined following Madsen and Wood (2002) for the wave and current cases separately, S is the ratio of sediment density to water density. The acceleration due to gravity is g and D is the sediment diameter. The median grain size (D_{50}) is 0.125mm in the Bay.

The modified Shields diagram is used to determine the critical Shields parameter, $\psi_{cr} = 0.085$. The maximum current of 5 cm/s leads to $\psi_{current} = 0.003$ ($u_* = 0.0024 m/s$) which is more than an order of magnitude less than the critical Shields parameter, thus no sediment motion is expected. The design wave height of 0.14

m leads to $\psi_{wave} = 0.232\,(u_* = 0.0212 m/s)$ which is considerably higher than the critical Shields parameter, so sediment motion is expected.

This information suggests that the currents alone can not supply the Bay sediments to the marsh and that the waves can. Even for velocities as high as 20 cm/s the bottom stress due to currents alone is insufficient to initiate the motion of non cohesive sediment. The top layer of sediment accreting in the marsh consists of very fine material with a measured fall velocity on the order of 3 cm/hour. The fine material remains suspended long enough to be advected into the marsh without significant local resuspension.

7. BERM DESIGN

The wave conditions in the marsh are a function of the water depth, berm dimensions and incident wave character (height, period, and direction). The berm is optimized to allow as much wave energy into the marsh as possible without causing significant erosion. Study of similar marshes in Galveston Bay by Shafer et al. (2003) suggests that wave-induced marsh erosion would be minimal if $H_{20\%} \le 0.14m$. Hence, the design wave requirements in the marsh are defined as $H_{20\%} \le 0.14m$.

7.1 Wave Transformation Over The Berm

Wave height transformation is determined using refraction and shoaling (Vincent et al. (2002)) for a non-breaking wave (Equations 3, 4 & 5) and the energy flux equation for a breaking wave (Equation 6) (Smith (2002)).

$$H_1 = H_0 K_s K_r \quad \textbf{(3)}$$

$$K_s = \sqrt{\frac{C_{g0}}{C_{g1}}} \text{ is the shoaling coefficient} \quad \textbf{(4)}$$

$$K_r = \left(\frac{\cos(\theta_0)}{\cos(\theta_1)} \right)^{1/2} \text{ is the refraction coefficient} \quad \textbf{(5)}$$

$$\frac{d\left(H^2 h^{1/2} \right)}{dx} = -\frac{\kappa}{h}\left(H^2 h^{1/2} - \Gamma^2 h^{5/2} \right) \quad \text{for } H > H_{stable} \quad \textbf{(6)}$$

where H is the wave height (H_0 – offshore, H_1 – some other location), C_g is the group velocity determined from linear wave theory, θ is the wave angle, $H_{stable} = \Gamma h$ is

the stable wave height, h is the water depth, $\kappa = 0.15$ is the empirical decay coefficient and $\Gamma = 0.4$ is an empirical coefficient. The energy flux equation is solved using finite differences for breaking waves applying linear shallow water theory assuming that the energy dissipation is proportional to the difference between local energy flux ($E*C_g$) and stable energy flux ($E*C_{g,s}$) (Smith (2002)).

Smith (2002) recommends equations for the breaker index (γ_b) (Equations 7-10). They are solved iteratively to determine the location of incipient breaking.

$$\gamma_b = \frac{H_b}{h_b} \quad \textbf{(7)}$$

$$\gamma_b = b - a\frac{H_b}{gT^2} \quad \textbf{(8)}$$

$$a = 43.8\left(1 - e^{-19\tan(\beta)}\right) \quad \textbf{(9)}$$

$$b = \frac{1.56}{1 + e^{-19.5\tan(\beta)}} \quad \textbf{(10)}$$

where $\tan(\beta)$ is the beach slope, H_b is the wave height at breaking, and h_b is the water depth at breaking. Equations 3, 4, and 5 are solved on a grid with 0.1 m spacing from the Bay towards the marsh. The breaker index is then calculated using both Equations 7 and 8. When both equations for the breaker index are approximately equal, the location of incipient breaking is reached. The energy flux method is then used to determine the wave height profile from the breaking point until the stable wave height is reached. After which refraction and shoaling begin again. It is assumed that the wave angle after breaking is normal to the berm.

7.2 Berm Design Characteristics

Different berm elevations and top widths were considered to determine the optimum design. The water level and wave conditions were input to the wave transformation model to determine the wave conditions in the marsh. The wave height data is analyzed with respect to percent occurrence to obtain a new average wave condition for each direction and speed. The effect of water depth in the Bay on wave height is considered by adjusting for its effect in the SWAN model and correcting the incident wave heights accordingly.

The wave height in the marsh is calculated for every water level in the -1 m to +1 m MLW range using 5 cm spacing for each of the wave conditions (5 wind speed bins and 12 direction bins). The marsh wave height is then weight averaged by its percent occurrence to determine the mean wave condition in the marsh for each water level. This results in a new transmitted wave height in the marsh for each direction/speed bin. The new wave distribution is used to calculate the 20% exceedence wave height in the marsh. Any berm design conditions which result in a 20% exceedence wave condition in the marsh of 0.14 m or below will be considered viable.

The results indicate as expected, that as the berm elevation is increased the 20% exceedence wave height in the marsh decreases. Table 2 lists the 20% exceedence wave height as a function of the berm top elevation with a 1/500 side slope and a 100 m top width. The top width and side slope have little effect on the transmitted wave heights predicted in this formulation. The waves needed to transport the sediment occur during times with lower than average water levels so the lower berm top elevations give the desired results. The existing bottom elevation in the marsh complex is about -0.4 m MLW so the -0.3 MLW top elevation is the lowest practical elevation.

Table 2: 20% exceedence wave height per berm top elevation.

Berm top elevation above MLW (m)	$H_{20\%}$ (m)
0.1	0.03
0	0.04
-0.1	0.05
-0.2	0.08
-0.3	0.1

The new wave conditions are then considered with respect to the expected average nourishment needs of the marsh. The section of marsh that this berm is intended to nourish requires an additional 2000 m^3/year to keep pace with relative sea level rise. The berm needs to supply at least four years of material to maintain a reasonable nourishment interval and to account for error and sediment losses. The berm top elevation of -0.2 m is chosen as the design. It allows the berm to meet the sediment volume requirements and allows for some erosion without affecting performance.

8. HYDRODYNAMIC MODEL INCLUDING THE BERM

The berm top width, elevation and side slopes were used to modify the bathymetry input to the marsh scale circulation model described in Section 4. Depth averaged velocity around the marsh was unchanged except above the berm. The model velocity above the berm is as high as 25 cm/s when the water level is within a few cm of the berm top. Velocity on the berm is probably over predicted when the water is very shallow above the berm.

The extreme velocity on the crest is mitigated by placing a channel through the berm, allowing the water to flow around the berm easily. The channel ensures that the extreme velocities will not occur on the berm. A cross section normal to the berm is plotted in Figure 7. The distances along this cross section are used to reference transport across the berm. The Bay is towards x = 0 and the marsh is towards x = 900.

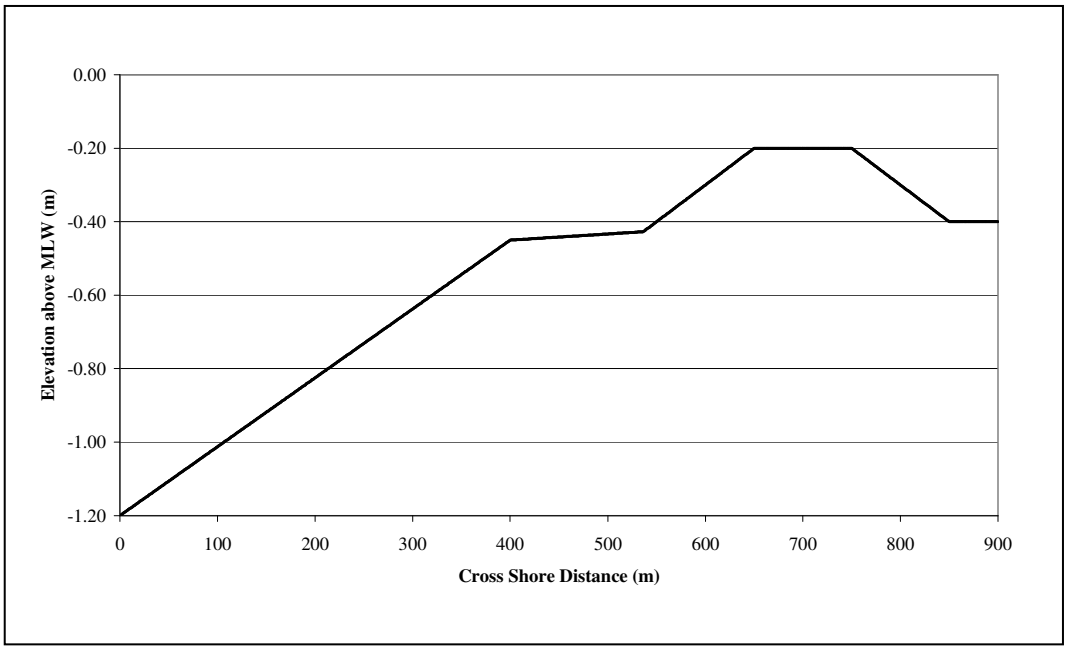

Figure 7: Simplified cross section of the berm.

Velocity is output from the RMA2 model at 5 cross-shore locations. The maximum velocity in the Bay is typically less than 5 cm/s. Velocity in the marsh away from the berm or entrances is also typically less than 5 cm/s. The velocity over a 7 day period is plotted in Figure 8 for the conditions when the wind is from 300º. The cross shore locations of velocity measurement correspond with the cross-shore distance in Figure 7. The plotted velocity is the 4 hour average which will be used in the transport model.

The pink line (x = 700) in Figure 8 is the velocity in the middle of the berm. The maximum velocity occurs over the berm. The dark blue and light green lines indicate the velocity on the Bay and marsh side of the berm, respectively. The purple and light blue lines indicate the velocity in the Bay and the marsh away from the berm.

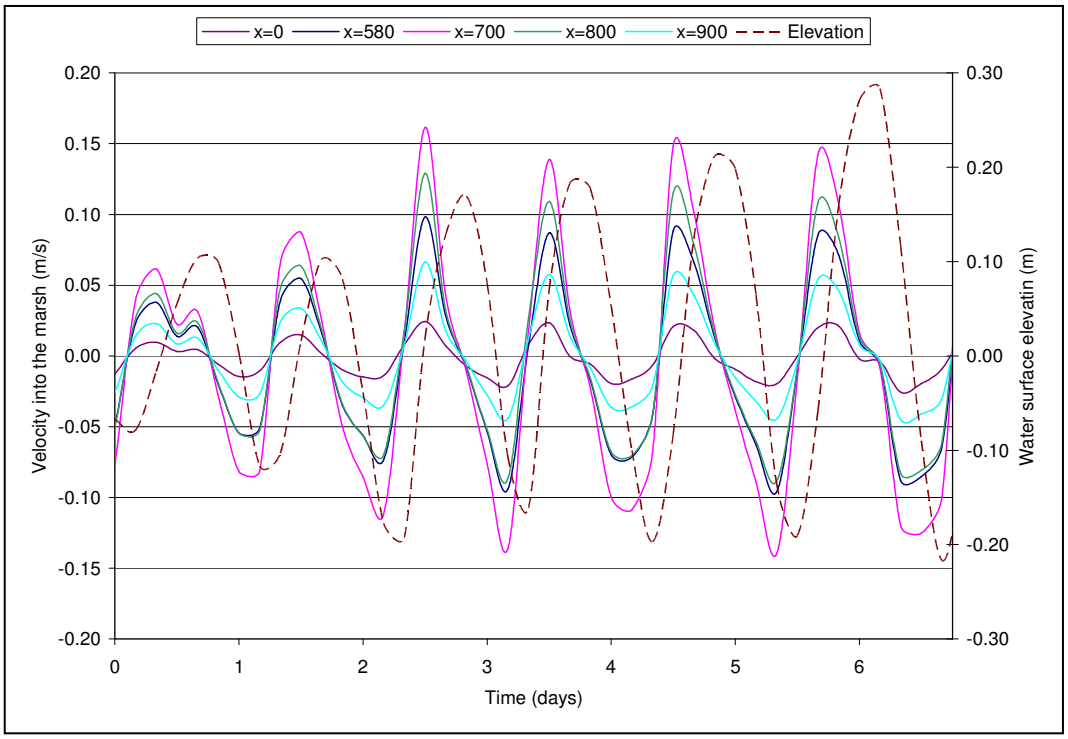

Figure 8: Water velocity and elevation when the wind is from 300º.

9. SEDIMENT TRANSPORT MODELING

This model of sediment transport is meant as a first approximation to the long term effects on the berm with its ultimate goal being to determine the annual rate of sediment supply to the marsh. The calculations are made assuming that the berm does not change. An infinite supply of sediment in the bed without natural erosive armoring of the bed is assumed.

Since the waves are so often nonlinear as they pass over the berm and into the marsh, a model which includes those effects must be employed to determine the net transport. The waves acting on the berm are short period with low wave heights (generally less than 2 seconds and 0.2 m in the Bay). These types of waves have rarely been specifically studied, so methods developed for open beaches and the continental shelf were adapted. Short waves in shallow water tend to act like deep water or transitional waves only becoming shallow water waves near breaking.

Transport is assumed to occur in two modes; bed load and suspended load. The case for breaking waves is handled by empirical extension of the non-breaking wave method for both bed load and suspended load. Bed load and suspended load are both enhanced in the direction of wave propagation for nonlinear waves. The effects of wave-current interaction also skew the transport in the direction of wave propagation.

9.1 Non-Breaking Wave Transport

Under most wave and water level conditions, waves do not break as they cross the berm and enter the marsh complex. Breaking only occurs for statistically large waves or low water levels. One dimensional (cross-shore directed) transport per unit width is calculated using Equation 11.

$$q(t) = \int u(z,t)C(z,t)dz \qquad \textbf{(11)}$$

$$q(t) = \int u(z,t)C(z,t)dz$$

where q(t) is the transport rate per unit width, C(z,t) is the vertical distribution of sediment concentration, and u(z,t) is the vertical distribution of horizontal velocity.

9.1.1 Suspended Load Concentration Profile

The concentration profile is determined by solving the sediment diffusion equation in one vertical dimension (Equation 12) using a finite difference approach.

$$\frac{\partial C_i}{\partial t} = w_{s,i}\frac{\partial C_i}{\partial z} + \frac{\partial\left(K_s \partial C_i\right)}{\partial z^2} \qquad \textbf{(12)}$$

where C_i is the concentration in a particular size class, $w_{s,i}$ is the measured mean fall velocity of each sediment size class and K_s is the vertical sediment diffusivity. The sediment diffusivity includes the effects of the wave and current induced vertical mixing. Madsen and Wood (2002) recommend a diffusivity that is a function of elevation and shear velocity for combined wave-current flows on the continental shelf. Ogston and Sternberg (2002) noticed that under non-breaking waves sediment diffusivity was vertically constant above twice the combined wave-current boundary layer. The sediment diffusivity here is assumed to be vertically constant (Equation 13) realizing that the diffusivity might be underestimated very near the bottom.

$$K_s = \kappa u_{*m} A_3 \qquad \textbf{(13)}$$

where u_{*m} is the combined wave-current shear velocity determined using the method provided by Madsen and Wood (2002) for a combined wave-current flow. Their method is modified to include the bottom slope through the modified Shields parameter employed by Baldock et al. (2005) and Fredsøe and Deigaard (1992). (Equation 14). κ is Von Karman's constant and A_3 is a constant determined to be equal to 0.03 through the laboratory test described in the next section.

$$\psi(t) = \psi_{flat}(t)\left(1 - \frac{\tan(\beta)}{\tan(\phi)}\right)\cos(\beta) \qquad \textbf{(14)}$$

where $\psi_{flat}(t)$ is the instantaneous Shields parameter calculated assuming a flat bottom, β is the bed slope and ϕ is the friction angle (32º for sand). The top boundary condition used to solve Equation 12 is $\left(\frac{\partial C}{\partial z} = 0\right)$ at the still water line. The bottom boundary condition is a time varying reference concentration, C_{ref}, (Equation 15) based on the bottom stress and the empirical resuspension parameter.

$$C_{ref}(t) = \gamma C_b F_i \left(\frac{|\tau(t)|}{\tau_{cr}} - 1\right) \text{ when } \psi(t) > \psi_{cr} \text{ otherwise } C_{ref} = 0 \qquad \textbf{(15)}$$

where $\gamma = 1.25 * 10^{-4}$ is the resuspension parameter determined through the laboratory test, C_b is the non-dimensional bed concentration equal to 0.65 and F_i is the fraction of sediment per size class present in the bed. $\tau(t)$ is the instantaneous bottom shear stress. The critical bottom shear stress, τ_{cr}, is calculated with Equation 16 (Madsen and Wood (2002)).

$$\tau_{cr} = \psi_{cr} g D_i \left(\rho_{sediment} - \rho_{fluid}\right) \quad \textbf{(16)}$$

where D_i is the median diameter of the size class, $\rho_{sediment}$ is the density of the sediment and ρ_{fluid} is the density of the fluid.

9.1.1.1 Bottom Shear Stress

Determination of the bottom shear stress is the first place the nonlinearity of the waves is considered. Myrhaug and Holmedal (2003) present a method for calculating the bottom stress to include the effects of regular second order Stokes waves. That method is reiterated and applied with the wave friction factor calculated empirically based on Equation 17.

$$f_w = r\,\mathrm{Re}^{-s} \text{ for } \mathrm{Re} < 3*10^5 \quad \textbf{(17)}$$

where r and s are empirical factors equal to 2.0 and 0.5 respectively. Re is the Reynolds number $\left(\frac{U_{wave} A}{\upsilon}\right)$. U_{wave} is the maximum bottom velocity predicted by linear wave theory. $A = \frac{U_{wave}}{\sigma}$ is the near bed orbital displacement and $\sigma = \frac{2\pi}{T}$, where T is the wave period and υ is the kinematic viscosity of the fluid. The wave only shear stress is $\tau_{linear} = \frac{\rho}{2} f_w U_{wave}^{\ 2}$.

Myrhaug and Holmedal (2003) then present a stress asymmetry factor (Equation 18) based on regular second order Stokes waves which represents the addition to the bottom stress at the second harmonic above the linear bottom stress. k is the wave number.

$$\Delta = \left[2 - 2\left(1 - \frac{1}{\pi}\right)s \right] \frac{3kH}{4\sigma \sinh^3 kh} \qquad \text{for } \Delta \le 0.2 \qquad \textbf{(18)}$$

The method presented by Myrhaug and Holmedal (2003) was developed for the case of asymmetric waves on a plane bed without current. The addition of the current does not change the form of Equation 18 but it does change the wave number due to wave current interaction (described in Section 9.1.3). The wave contribution to the instantaneous bottom stress (Equation 19) is then determined based on the maximum bottom induced stress, τ_{linear} .

$$\tau_{wave}(t) = \tau_{linear}\left(\cos(\sigma t) + \Delta\cos(2\sigma t)\right) \qquad \textbf{(19)}$$

τ_{linear} is calculated with linear wave theory for the wave only case following the method presented by Myrhaug and Holmedal (2003). Madsen and Wood (2002) developed a method to calculate the bottom stress due to waves and currents for the combined flow. They suggest a method to solve iteratively for the combined friction factor. The maximum wave induced shear velocity, current induced shear velocity and combined shear velocity result from this approach. The bottom stresses due to waves and currents are then calculated with Equation 20.

$$\tau = \rho_{fluid} u_*^{\,2} \qquad \textbf{(20)}$$

The new wave induced shear velocity in the presence of the current is used in Equation 20 to determine a new τ_{linear} and $\tau_{wave}(t)$. The instantaneous magnitude of the wave and current induced bottom stress is calculated with Equation 21.

$$\tau(t) = \sqrt{(\tau_{wave}(t))^2 + \tau_c^{\,2}} \qquad \textbf{(21)}$$

9.1.2 Laboratory Test to Calibrate Suspended Concentration

A laboratory test was conducted in a wave flume (Figure 9) at Texas A&M at Galveston to estimate how much sediment waves acting on a submerged berm can transport. The water depth in the wave flume varied between 15 and 30 cm. The wave flume is 40 cm wide and 8 m long. The test consisted of material collected in Galveston Bay near the State Park submerged in the wave tank being acted on by small waves at full scale (over the berm section of the marsh).

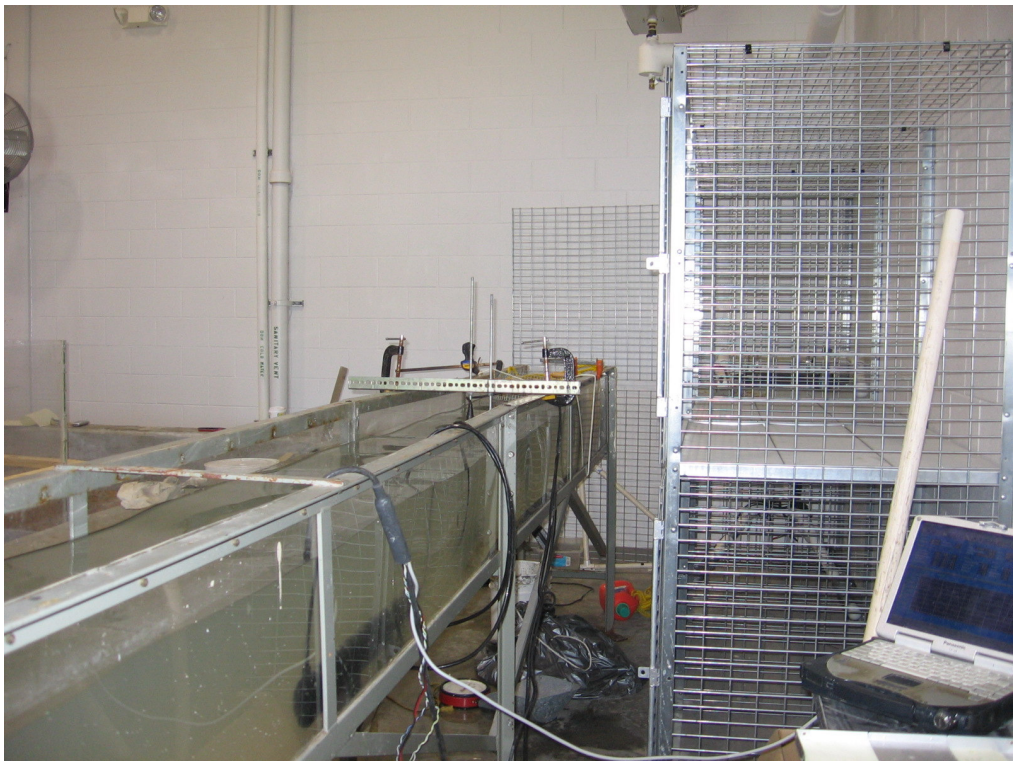

Figure 9: Wave flume.

The lab tests provided the data required to calibrate the sediment transport model for non-breaking waves. The best fit of the calculated concentration with the measured concentration was determined by varying the resuspension parameter and the diffusivity constant. Three wave heights and two water depths were used for 6 tests for both the native bed (D_{50} = 0.125 mm) and washed bed (D_{50} = 0.170 mm). The washed bed consists of native sediments made to have a coarser grain size distribution by rinsing the native bed to remove the fines. The fines were removed from the native bed in order to more easily measure the transport of sand.

Concentration was measured 3.5 cm and 8 cm above the bottom using optical backscatter sensors (OBS) calibrated by filtering collocated water samples. Measured concentrations ranged from 0.01 g/L to 1.0 g/L and the OBS's were calibrated linearly with a squared correlation coefficient of 0.91. A Laser In-Situ Scattering and Transmissometry (LISST) device was used to measure the suspended grain size distribution during different wave events. This instrument provides the ability to determine the fraction of different sized sediments in suspension rapidly (LISST ST Particle Size Analyzer User Manual), a factor also predicted by the transport model.

The velocity is measured 8 cm above the bottom using an Acoustic Doppler Velocimeter, a Nortek Vector and is used to determine the wave height and period in the flume. The LISST was used to measure the grain size distribution of the native and washed bed (Figure 10) and to measure the distribution of sediment suspended 12 cm above the bottom under different wave conditions (Figure 11). Figure 11 is a plot of the suspended grain size distribution as a function of the maximum near bottom velocity. The variation in suspension of coarse particles is sensitive to increases in the near bottom wave induced velocity.

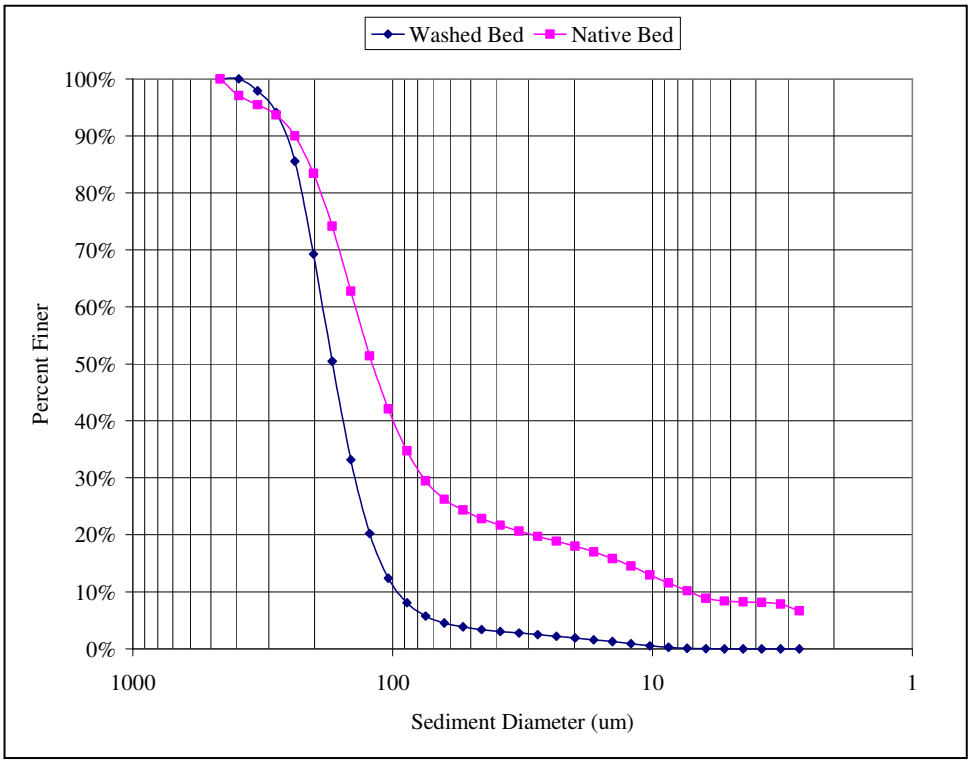

Figure 10: Grain size distribution of bed sediments.

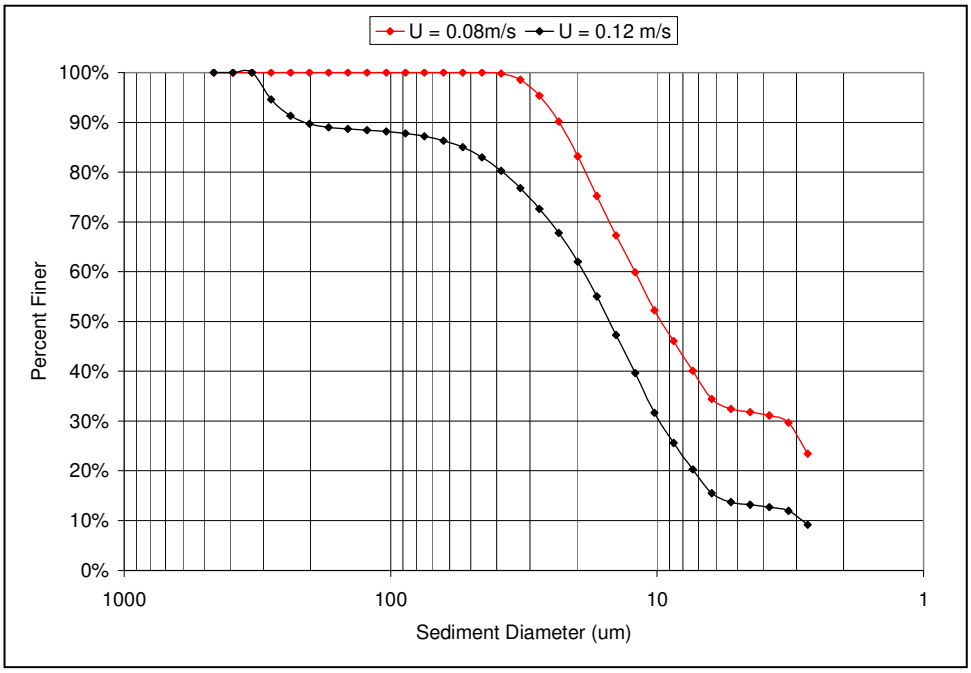

Figure 11: Suspended grain size distributions as a function of maximum near bottom velocity.

Observation of the velocity profile revealed that the waves in these shallow conditions were not well modeled with linear wave theory. However, Stokes second order wave theory predicted the velocity profile very well for all conditions in the wave flume. A comparison between the measured velocity and both wave theories is shown in Section 9.1.3. Further analysis of the natural conditions showed that the second order wave theory is valid in nature for the entire domain, excluding a region surrounding the surf zone.

Figure 12 plots the measured results from the wave flume experiments compared with the model predictions of concentration in the wave flume. A squared correlation coefficient of 0.92 was found with this data after one outlying test was removed. This calibration is conducted in a wave only case because the wave flume is not capable of producing currents. Soulsby and Damgaard (2005) state that there has been no study to verify the case of asymmetric waves and currents. No new data to the contrary has been found.

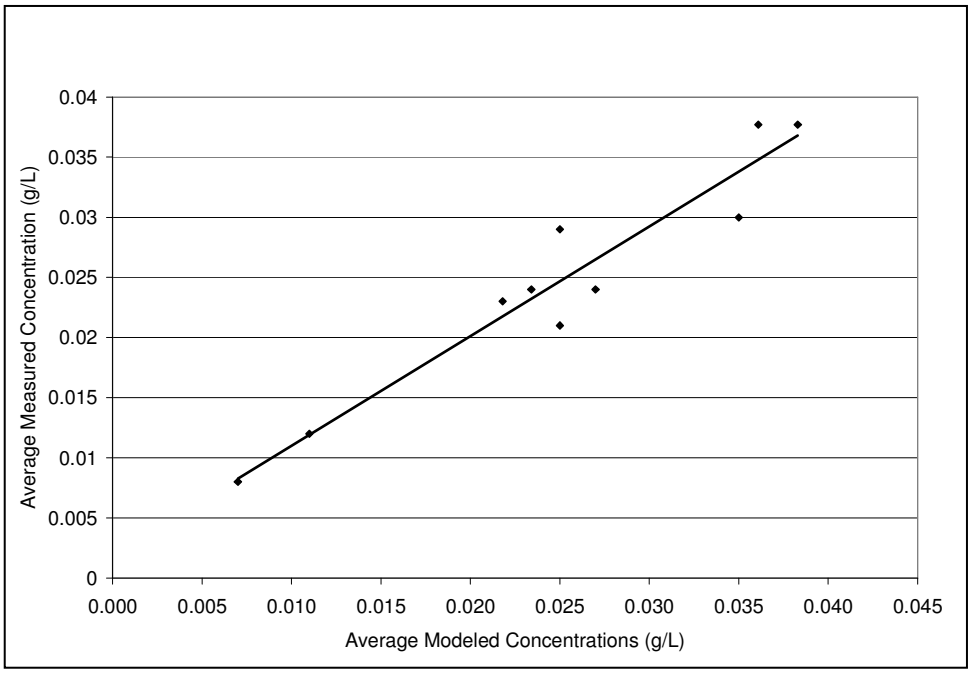

Figure 12: Comparison of modeled vs. measured suspended concentration.

9.1.3 Velocity Profile

Horizontal velocity (Equation 22) is calculated with potential flow theory expanded to second order. The solutions presented by Sobey (1997) for regular waves over a horizontal bottom in the steady frame with a constant current are used.

$$u(z,t) = U + \left|\cos(\theta_{wc})\right| \left(\frac{g}{k}\right)^{1/2} \left[\varepsilon A_{11} \frac{\cosh(k(h+z))}{\cosh(kh)} \cos(\sigma t) + 2\varepsilon^2 A_{22} \frac{\cosh(2k(h+z))}{\cosh(2kh)} \cos(2\sigma t) \right] \quad \textbf{(22)}$$

$$\varepsilon = \frac{kH}{2} \quad \textbf{(23)}$$

$$A_{11} = (\tanh(kh))^{-1/2} \quad \textbf{(24)}$$

$$A_{22} = \frac{3}{8}\left((\tanh(kh))^{-4} - 1\right)(\tanh(kh))^{1/2} \quad \textbf{(25)}$$

where θ_{wc} is the angle between the wave and current. The current, U, is assumed to be vertically constant and equal to the depth averaged current calculated with RMA2 and k is determined with the dispersion relationship (Equation 26).

$$\frac{2\pi/k}{T} = \left(\frac{g}{k}\right)^{1/2} \left[C_0 + \varepsilon^2 C_2\right] + U \quad \textbf{(26)}$$

$$C_0 = (\tanh(kh))^{1/2} \quad \textbf{(27)}$$

$$C_2 = \frac{1}{16}\left(9 - 10(\tanh(kh))^2 + 9(\tanh(kh))^4\right)(\tanh(kh))^{-3.5} \quad \textbf{(28)}$$

The velocity in the wave flume during the lab tests was collected at a sufficient rate (8 Hz) to compare the modeled wave induced velocity with the calculated velocity. Figure 13 plots the measured horizontal velocity 8 cm above the bottom in the wave

flume against the predicted velocity using linear wave theory and the second order Stokes wave theory. The wave height was 3.5 cm for this test with a period of 1.9 s in a water depth of 22 cm. These conditions occur on the berm during a typical tidal cycle. The plot shows that small waves in shallow water are well approximated by the second order Stokes theory.

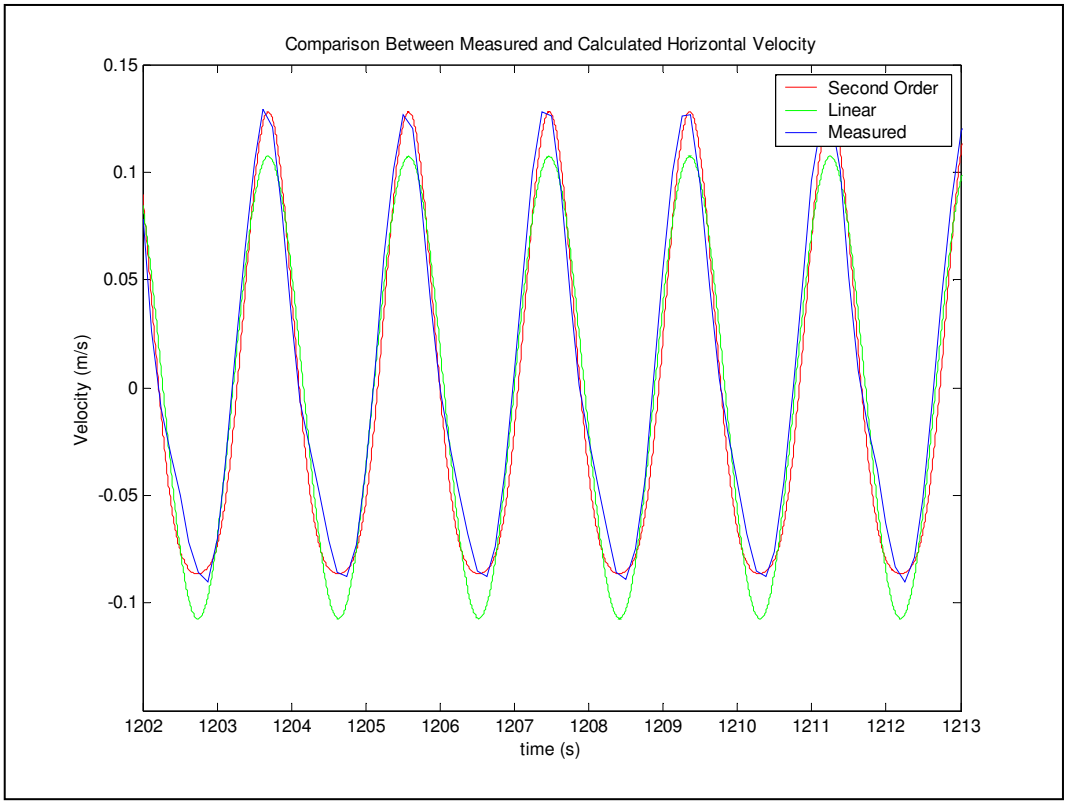

Figure 13: Comparison between measured and calculated velocity in the wave flume.

The wave contribution to the horizontal velocity is transformed into its component velocity in the direction of the current. This procedure is an ad-hoc method that reduces the net transport in the direction of the current due to the waves when the waves and current are not aligned.

The wave theory is stretched in the region near breaking. When the water depth becomes too shallow for the dispersion relationship developed by Sobey (1997), the calculated wave length will become large. When this begins, the linear dispersion relationship is substituted as part of the process to stretch the wave theory to a shallower region.

9.1.4 Suspended Load Transport Calculation

The sediment is split into four size classes for solving the problem. The percent of each size class is determined by analyzing the bed composition using the LISST and wet sieving many samples across the Bay. Table 3 lists the average results of the Bay bottom composition. Fall velocity was measured with the LISST. Calculating suspended sediment transport is a simple matter of numerically integrating Equation 11. Each of the 4 sizes classes are then summed to determine the total transport after the concentration and velocity profiles have been determined.

Table 3: Composition of Bay Sediments.

Diameter (μm)	Percent of Bed Composition	Fall Velocity (cm/s)
0 - 50	15%	0.04
50 - 100	11%	1.3
100 - 150	34%	1.7
> 150	40%	2.3

9.1.5 Bed Load

Bed load transport is calculated directly following the work of Soulsby and Damgaard (2005). The method they present includes the effects of currents and asymmetric waves. The asymmetry is accounted for with the same Δ defined in the suspended load section. This method was developed for predominantly large sand beds. Soulsby and Damgaard (2005) found that 62% of predictions were within a factor of 2 of the measured values for asymmetric waves without a current. They do not present a comparison of predictions against data for the case of asymmetric waves in the presence of a current. Likewise, an attempt at quantifying the accuracy of this bed load transport application in the presence of currents was not attempted. Bed load transport was compared with suspended load to ensure that it was no more than an order of magnitude greater.

The equations presented by Soulsby and Damgaard (2005) for calculating bed load transport due to currents and asymmetric waves are reproduced for clarity (Equations 29 – 33).

$$\Phi = \frac{q_b}{\sqrt{g(S-1)D^3}} \quad \textbf{(29)}$$

$$\Phi_{x1} = A_2 \psi_m^{1/2} (\psi_m - \psi_{cr}) \quad \textbf{(30)}$$

$$\Phi_{x2} = A_2 (0.9534 + 0.1907 \cos(2\theta_{wc})) \psi_w^{1/2} \psi_m + A_2 \left(0.229 \Delta \psi_w^{3/2} \cos(\theta_{wc})\right) \quad \textbf{(31)}$$

$$\Phi_x = \max(\Phi_{x1}, \Phi_{x2}) \quad \textbf{(32)}$$

$$\Phi_y = A_2 \frac{\left(0.1907 \psi_w^{\,2}\right)}{\psi_w^{3/2} + \left(\frac{3}{2}\right) \psi_m^{3/2}} (\psi_m \sin(2\theta_{wc}) + 1.2 \Delta \psi_w \sin(\theta_{wc})) \quad \textbf{(33)}$$

where Φ is the dimensionless bed load transport rate with the x axis in the direction of the current and q_b is the dimensional bed load transport rate. Φ_x is the non

dimensional transport rate in the direction of the current and Φ_y is normal to the current. The subscript m and w on the Shields parameters indicate the mean and wave induced components. They are taken to be the current and wave induced values respectively. A_2 is an empirically determined parameter found to be 12 by Soulsby and Damgaard (2005). These equations were taken directly from Soulsby and Damgaard (2005) and the reader is referred to their work for more detail.

The bed load transport is determined using sediment properties of the median grain size. The same method of calculating the skin friction shear stress in the suspended load section (Section 8.1.1.1) is used to determine the motivating stress on the bed load. The only modification made is in the determination of the Shields parameter (Equation 15) to include the effects of bed slope.

9.2 Breaking Wave Transport

Transport under breaking waves is handled by empirical extension of the non-breaking wave case. A limited amount of data was collected in Galveston Bay on 27 October 2006 in a location with similar sediment and bathymetric characteristics to the submerged berm analyzed here. The modifications to the non-breaking wave transport are discussed here but the entire procedure is not reiterated.

9.2.1 Velocity Profile

Comparison between the limited collected data set and one wave only case of barrier island overtopping is presented as limited verification. Visual observation of waves breaking under conditions similar to the case studied here indicates that the breaking wave will maintain its non-breaking shape with the addition of a surface roller. Svendsen (1984) notes that the surface roller can be considered as an additional volume of water carried with the wave, increasing the total volumetric flux. Srinivas and Dean

(1996), while studying overtopping of a barrier island, simplified the augmented volumetric flux presented by Svendsen (1984). They calculate volumetric flux by extending linear theory to second order and multiplying by a coefficient, F_m (Equation 34).

$$F_m = \left(1 + \frac{7kh}{2\pi}\right) \quad \textbf{(34)}$$

Data collected under breaking waves on 27 October 2006 in an area of the Bay that simulates the expected conditions over the berm indicates a 47% increase in the time mean velocity beyond that calculated with the second order Stokes approximation. The water depth during the data collection was 0.45 m with a breaking wave height of 0.21 m and a period of 2 s; conditions beyond the validity of the second order approximation. The measured velocity was corrupted so the validity of the measured mean velocity is questionable.

The net flux is directly related to the net velocity under the wave so the increased volumetric flux should result in an increased net velocity. F_m will be used as an empirical parameter to modify the wave characteristics used for non-breaking. The second order approximation is stretched to the breaking region by multiplying the wave velocity by the factor F_m. The breaking velocity will increase with increased breaking depth and, by association, with increased breaking height. The breaking velocity will be decreased by increased wave length. Steeper waves during breaking will have increased velocities.

F_m was approximately 1.8 for the conditions measured on 27 October 2006. The limited variation in the wave conditions at the project site ensures that F_m will be approximately the same for all expected cases. The advantage to using a variable amplification factor is that some of the variable character due to wave steepness is captured. When the second order predicted velocity is modified the net calculated

velocity is 2% below the measured net velocity. More data needs to be collected for rigorous verification.

The velocity solution will become unrealistically large in very shallow water. The solution is stretched until $\Delta > 0.25$ but as the solution becomes unusable the velocity is reduced to the current only case. Wave-current interaction is handled in the same manner as the non-breaking case.

9.2.2 Suspended Load Concentration Profile

Srinivas and Dean (1996) developed a model of vertical diffusivity under breaking waves. They make the connection between the dissipation of turbulent kinetic energy and the increase of bottom shear stress and sediment diffusivity, assuming that the turbulence generated at the surface penetrates the entire water column. The breaking waves we are examining are small, short period waves that have a small intermittent roller on the surface. The waves can be described as spilling except when the water level is low enough for the waves to break directly on the berm.

During breaking the sediment diffusivity will retain the form of Equation 13. The increase in mixing will be captured by multiplying the maximum near bottom velocity, calculated with linear wave theory, by a factor F_m when calculating the shear velocity. Srinivas and Dean (1996) also use a depth averaged eddy viscosity but they account for the increase in bottom stress in a different fashion. They describe an additional shear velocity which is a function of the dissipation of turbulent kinetic energy.

The suspended sediment concentration was measured at 8 cm and 18 cm above the bottom with concentrations of 0.67 g/L and 0.43 g/L respectively on 27 October 2006. Bed sediment was analyzed at 1 location where the breaking wave data was collected. The sediment was coarser than the sediment found in West Bay (D50 = 0.144 mm) with 5 % less fines. The model concentration was calculated, based on the observed water depth, wave height and wave period, at 8 cm and 18 cm above the

bottom as 0.54 g/L and 0.33 g/L respectively. The calculated concentration under the breaking wave is approximately 20% less than measured.

The model of suspended concentration is sensitive to the bed concentration. The suspended concentration at the measurement location is a function of the average bed composition in the surrounding area. Using the average sediment composition found in West Bay (Table 3) increases the calculated concentration to 0.67 g/L 8 cm above the bottom and 0.44 g/L 18 cm above the bottom.

9.2.3 Breaking Wave Transport Calculations

The suspended load and bed load are calculated in the same manner as the non-breaking wave case employing the stated assumptions. It is expected that the transport during the brief time of extremely low water level could be very large if the flow was forced over the berm. The marsh complex is designed with many entrances making the importance of this phenomenon less likely to be significant. Furthermore, it is possible that a channel will develop in the berm naturally and the artificial addition of such a channel will reduce the current velocity over the berm.

A special case is encountered as the water level drops below the sacrificial berm. The solution is stopped as the water depth drops below 2 cm on the berm. Significant long shore transport could occur when the waves break directly on the berm but the long shore transport isn't considered here. This effect could reduce the nourishment interval significantly and cause sedimentation problems down drift.

A comparison of cross-shore transport between the preceding model of breaking transport and the same domain without the modified velocity was made to quantify the effects of the empirical extension. The percent increase in transport caused by the empirical extension is shown in Table 4 for the water level at MLW. The cross shore transport due to a 0.2 m wave normal to the berm with a 2 s period is plotted in Figure 14. The figure shows the addition to transport caused by the empirical breaking scheme.

The maximum increase to transport caused by the empirical breaking was approximately 20%.

Table 4: Increase in transport due to modified velocity as a function of current.

U (m/s)	H (m)	T (s)	Increase in Transport due to Modified Velocity
-0.1	0.2	2	24.0%
-0.05	0.2	2	13.3%
0	0.2	2	13.0%
0.05	0.2	2	12.6%
0.1	0.2	2	10.1%

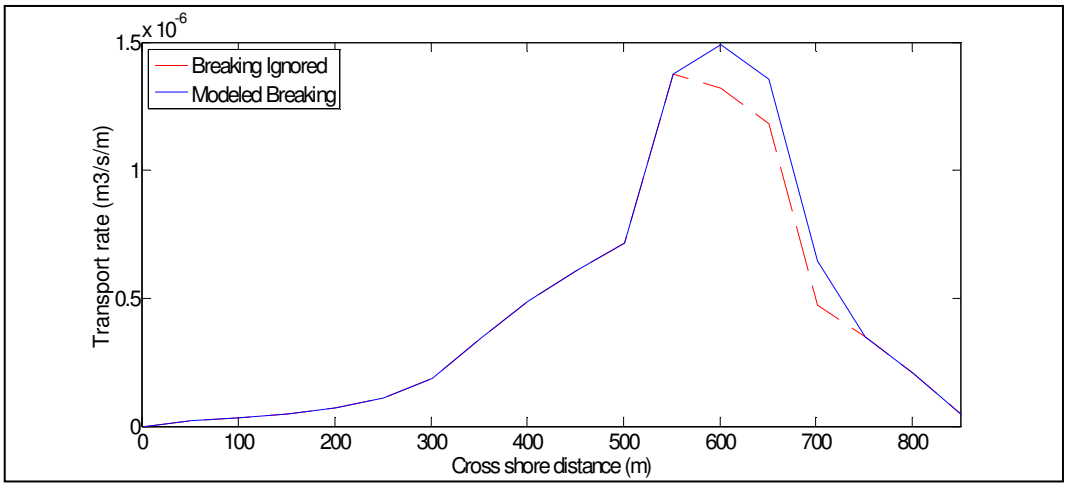

Figure 14: Cross shore transport with and without empirical breaking.

9.3 Net Transport Calculation Method

The model of cross-shore transport calculates the net sediment transport for any given wave and current conditions. The goal of the transport model is to estimate the net transport of sediment into the marsh complex and the rate at which the berm needs to be nourished. This analysis will assume that the shape of the berm is constant. The increased transport into the marsh is estimated and qualitative judgments about berm evolution are made. A future application will be to link all of the models allowing the bed to change employing the sediment continuity equation (Equation 35).

$$\frac{\partial q}{\partial x} = -\frac{\partial h}{\partial t} \qquad \textbf{(35)}$$

The solution is calculated for each wind direction, wave height and water level. Each simulation consists of one half of the spring neap tidal cycle around the mean water level for each wind direction. The steady solution is obtained for each 4 hour period. The mean of the solutions is the net transport rate per environmental condition. The transport rate for the entire year assuming no change in bed elevation is then recorded. The net transport rate during each set of environmental conditions is multiplied by its percent occurrence and then all conditions are summed.

A three point moving average is applied to the transport rate over the horizontal domain. The smoothing process reduces the maximum transport and moves the location of maximum transport slightly shoreward for the wave only case. The smoothing process also artificially adds some advection and dispersion to the solution.

9.3.1 Comparison of Wave-Only Net Cross Shore Transport

The cross-shore transport was calculated for a wave only case to visualize the net transport caused by waves and to investigate the effect of water level on transport (Figure 15). A 20 cm wave with a 2 s period in the Bay was used to calculate the transport across the berm under five different water level conditions. The water level is listed as depth in cm on the berm. The center of the berm is located at 700 m and the Bay is at 0 m. The transport increases as the depth decreases and it is obvious that as the depth on the berm approaches 0, the transport solution will be invalid.

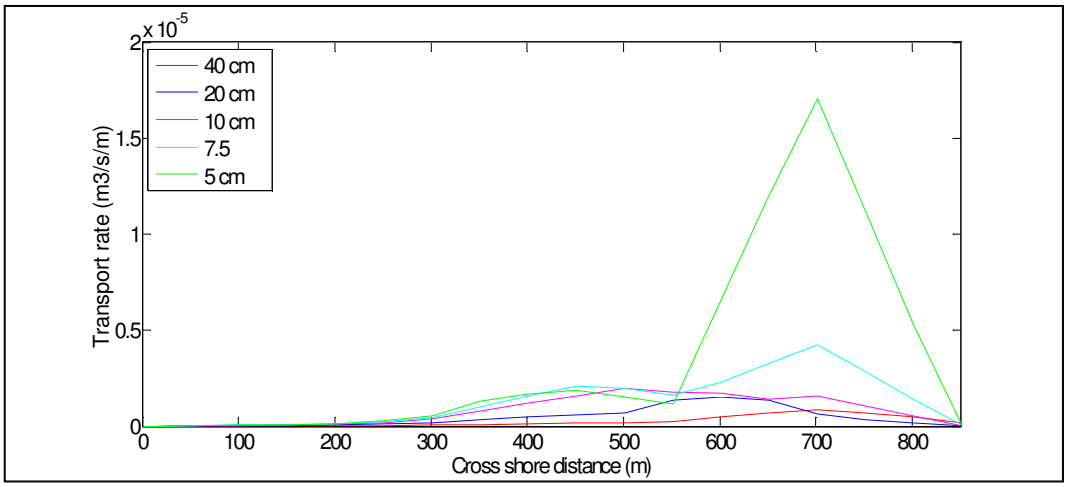

Figure 15: Cross-shore transport caused by waves only.

The most similar case found in the literature to the problem examined here is the model test of barrier island overtopping made by Srinivas and Dean (1996). The model wave characteristics they use are a 16 cm wave with a 2 s period and a nominal inundation of 10 cm. They calculate the deposition of sand over the island at a rate of approximately $3*10^{-7}$ $m^3/s/m$. The back of the berm, which would be a location similar to the location behind the crest of the island, is at 800 m in Figure 12. The calculated transport at 800 m for a 10 cm water depth above the berm for a 16 cm wave height with a 2 s period using this model is $2*10^{-7}$ $m^3/s/m$. These results show reasonable agreement with the case presented by Srinivas and Dean (1996) for a sandy barrier island during an overtopping event. The similar results lend confidence to this model of sediment transport for a case with breaking.

10. SEDIMENT TRANSPORT RESULTS

The net yearly transport over the submerged berm into the marsh is shown in Figure 16. The net transport in water deeper than approximately 0.6 m below MLW is zero because the waves in this region are typically linear and the currents are very low and symmetric. The current alone is not able to initiate motion of sediment larger than about 15 μm except on the berm when the water level is very low. Even when the current can initiate suspension the net transport is two orders of magnitude less than in the presence of waves. The calculated yearly net transport is the transport occurring when the waves are included; which is 34% of the time.

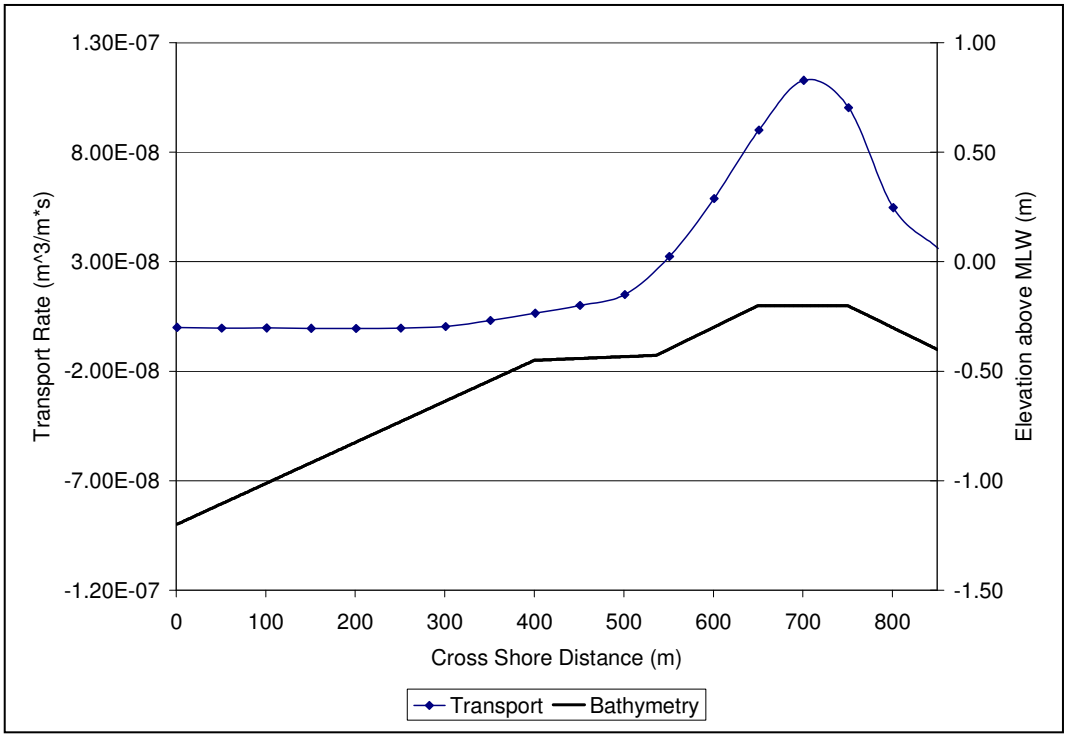

Figure 16: Cross shore variation of yearly net transport rate.

Since the marsh is currently accreting at a rate of 0.25 cm/year with no waves entering the marsh complex, the transport of fines (due to advection and dispersion) must be equivalent to that amount because the bottom stress in the marsh due to currents alone is insufficient to resuspend sediment. There is a significant supply of suspended fines during most of the year because waves in the Bay still initiate suspension of fine sediments. The fines are then transported into the marsh through advection and/or dispersion. Therefore, it is assumed that the existing rate of accretion is the background rate and that it will continue in the future as an addition to the transport due to waves.

The additional transport into the marsh is $3.6*10^{-8}$ $m^3/s/m$, the net transport at 850 m in Figure 13, which is equivalent to 1.14 m^3/year/m. The test case was a 550 m wide berm with a 40 m wide channel to reduce the effects as the water level was very near the berm crest. The test case provides an additional 630 m^3/year to the marsh increasing the accretion rate to approximately 0.38 cm/year. The berm can be extended to a width of 1200 m, increasing the accretion rate to approximately 0.52 cm/year. With the widest possible berm the sediment supply to the marsh will be doubled but still 0.13 cm/year short of the expected relative sea level rise.

Quantitative properties of the transport calculations can be used to make qualitative judgments about berm evolution. The gross transport over the berm is an order of magnitude higher than the net transport. This indicates that the berm will naturally spread in both directions, but be skewed toward the direction of wave propagation. The sediment continuity equation (Equation 35) relates the cross-shore variation of transport to the change in bottom elevation over time.

The small scale evolution of the berm is too computationally intense to calculate but the long term net transport rates can be used to determine the trend of berm evolution. The cross-shore variation in the horizontal derivative of transport rate is shown in Figure 17. Since $\frac{\partial q}{\partial x} > 0$ on the Bay side of the Berm and $\frac{\partial q}{\partial x} < 0$ on the marsh side, the berm will naturally propagate into the marsh. The currents will also play a role in smoothing the berm causing the top of the berm to tend towards being flat.

Figure 17: Cross-shore variation in the horizontal derivative of transport rate.

Figure 18 plots the shape of the designed berm compared to the shape of the berm predicted by the net transport after one year. The net berm evolution is toward the marsh.

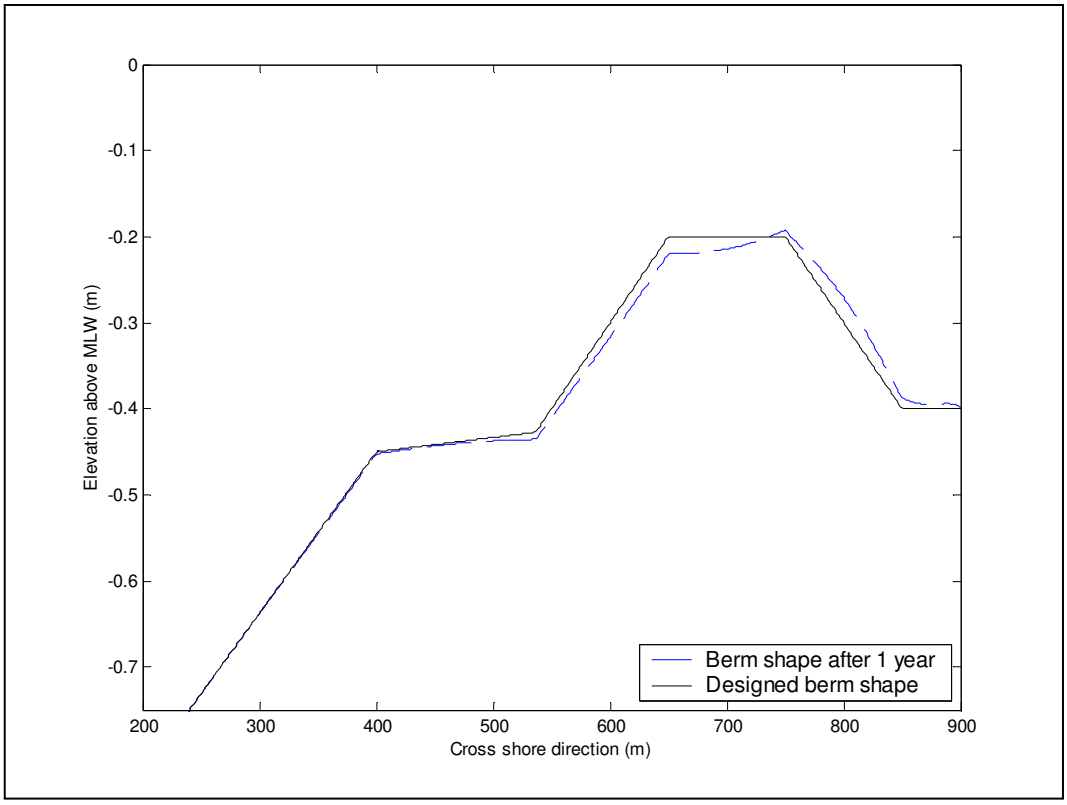

Figure 18: Net berm evolution after one year.

The volume of the 100 m wide (cross shore width) berm is 42 m^3/m. Assuming that the 1.14 $m^3/year/m$ of sediment transported into the marsh originates from the berm,

the berm will be completely exhausted in 36 years. The transport model employs many assumptions, so it is likely that the nourishment interval will be shorter. These results suggest that the berm width can be reduced by at least 50 m giving a maximum nourishment interval of about 18 years.

The data to rigorously verify this transport model is not available. Typically, the best results that can be expected from a sediment transport model are within a factor of two with error over an order of magnitude not being uncommon (Davies et al. (2002)). The lab test and field data collected are critical to minimizing the model error but a more detailed physical test of cross shore transport is required to verify the long term accuracy. The physical and time scale of this problem precludes the collection of that data at this stage but these results strongly support undertaking that task. A field demonstration project could determine the accuracy of the model and the feasibility of using this approach to increase sediment supply to a salt marsh.

11. CONCLUSION

The extreme loss of salt marsh in Galveston Island State Park is due primarily to submergence caused by relative sea level rise. The wave conditions in the marsh make it unlikely that wave-induced erosion was a primary contributor. All of the marshes on the Bay side of Galveston Island have experienced significant loss and this analysis suggests that the loss will continue in the future. The only currently employed method to mitigate marsh lost to submergence in Galveston Bay is the artificial creation of new marsh. The new marsh then experiences the same rate of loss to relative sea level rise as the natural marsh.

The submerged berm can successfully control wave transmission into the marsh and will increase sediment supply. The transport model indicates that the sediment supply to the marsh can be doubled by using a 1200 m submerged berm around the marsh complex. The model predicts that the nourishment interval will be a maximum of 18 years with a 50 m wide berm. This estimate does not include the effects of the berm spreading due to the high gross transport. It is expected that this nourishment interval is extreme and it is likely that the interval will be 2 or 3 times shorter.

The lab data suggests that the modeled concentration is accurate. The empirical extension to calculate transport under breaking waves only provides an additional 20% transport. This increase is lower than determined by Yu et al. (1993), but they were studying wave breaking on an Atlantic Coast beach. It seems reasonable that transport due to breaking conditions in the Bay would not be as greatly increased.

Even if the model error is only a factor of two, the benefits to the marsh are still directly dependent on the error. If the actual increased sediment supply is a factor of two higher, the design would be beneficial. However, if it is a factor of two lower, the design is not feasible. These results justify attempting a large scale physical model or a demonstration project in the field to more accurately quantify the potential gains. A demonstration project to determine the actual feasibility of this design will prove the concept and, if feasible, increase the sustainability of the demonstration project. The

demonstration project could result in much lower transport rates. In that case the berm could be constructed of finer material.

The primary benefit of using the sacrificial berm to increase sediment supply is in the environmental effectiveness of the marsh. No scientific determination as to whether or not an artificially created marsh can ever replace a natural marsh has been agreed upon (O'Connell 2003). This makes it imperative that a method to increase the natural marshes ability to resist relative sea level rise be developed.

REFERENCES

Baldock, Hughes, Day and Louys. 2005. Swash overtopping and sediment overwash on a truncated beach. Coastal Engineering, 52, 633-645.

Davies, Rijn, Damgaard and van de Graaff. 2002. Intercomparison of research and practical sand transport models. Coastal Engineering, 46, 1-23.

Donnell, Barbara P., Letter, Joseph V., McAnally, W. H., and others, "Users Guide for RMA2 Version 4.5," 22 April 2005, http://chl.wes.army.mil/software/tabs/docs.htp.

Fredsøe, J., Deigaard, R., 1992. Mechanics of Coastal Sediment Transport. Advanced Series on Ocean Engineering, vol. 3. World Scientific, Singapore.

Glass, P., Hollingsworth, T. 1999. "Wetlands Restoration at Galveston Island State Park a Multi-Agency Project ", Proceedings of the Galveston Bay Estuary Program State of the Bay Symposium IV, Moody Gardens Hotel & Convention Center, Galveston, TX, pp 201-204.

Harris Galveston Subsidence District. 28 August 2006. http://www.subsidence.org/.

HDR Shiner Moseley and Associates, Inc. 28 August 2006. http://www.shinermoseley.com/.

"LISST ST Particle Size Analyzer User Manual." 8 August 2005. Sequoia Scientific, Inc.

Madsen, O., and Wood, W. 2002. Sediment Transport Outside the Surf Zone. In: Glenn, S., Houston, J., Mclean, S., and Walton, T. (editors), Coastal Engineering Manual, Part III , Coastal Sediment Processes Chapter III-6 , Engineer Manual 1110-2-1100, U.S. Army Corps of Engineers, Washington, DC.

Myrhaug, D. and Holmedal, L.E. 2003. Laminar bottom friction beneath nonlinear waves. Coastal Engineering Journal, 45, 49-61.

NOAA Center for Operational Oceanographic Products and Services (CO-OPS). 28 August 2006. http://tidesandcurrents.noaa.gov/.

O'Connell, M.J. 2003. Detecting, measuring and reversing changes to wetlands. Wetlands Ecology and Management, 11, 397-401.

Ogston, A.S. and Sternberg, R.W. 2002. Effect of wave breaking on sediment eddy diffusivity, suspended-sediment and long shore sediment flux profiles in the surf zone. Continental Shelf Research, 22, 633-655.

Proosdij, D., Davidson-Arnott, R., Ollerhead, J. 2006. Controls on spatial patterns of sediment deposition across a macro-tidal salt marsh surface over single tidal cycles. Estuarine, Coastal and Shelf Science, 69, 64-86.

Santschi, Presley, Wade, Garcia-Romero, and Baskaran 2001. Historical contamination of PAHs, PCBs, DDTs, and heavy metals in Mississippi River Delta, Galveston Bay and Tampa Bay sediment cores. Marine Environmental Research, 52, 51-79.

Schwimmer, R.A., 2001. Rates and processes of marsh shoreline erosion in Rehoboth Bay, Delaware, U.S.A. Journal of Coastal Research, 17(3), 672-683.

Shafer, D. J., Roland, R., and Douglass, S. L. 2003. "Preliminary evaluation of critical wave energy thresholds at natural and created coastal wetlands," WRP Technical Notes Collection (ERDC TN-WRP-HS-CP-2.2), U.S. Army Engineer Research and Development Center, Vicksburg, MS. www.wes.army.mil/el/wrtc/wrp/tnotes/tnotes.html

Shiner, Moseley and Associates. 1998. Galveston Island State Park Marsh and Wetland Restoration: Preliminary Phase Report, Corpus Christi, TX.

Smith, J. M. 2002. Surf Zone Hydrodynamics. In: Dally et al.. (editors), Coastal Engineering Manual, Part II , Coastal Hydrodynamics Chapter II-4 , Engineer Manual 1110-2-1100, U.S. Army Corps of Engineers, Washington, DC.

Sobey, R.J. Course Notes. Linear and nonlinear Wave theory. 19 June 1997.

Soulsby, R. L. and Damgaard, J.S. 2005. Bedload sediment transport in coastal waters. Coastal Engineering, 52, 673-689.

Srinivas, R. and Dean, R.G. 1996. Cross shore hydrodynamics and profile response modeling. Coastal Engineering, 27, 195-221.

Svendsen, I.A., 1984. Mass flux and undertow in a surf zone. Coastal Engineering., 8: 347-365.

"SWAN User Manual." 4 September 2006. Delft University of Technology. http://www.fluidmechanics.tudelft.nl/swan/index.htm

Vincent, L.C., Demirbilek, Z. and Weggel, W. 2002. Estimation of Nearshore Waves. In: Dalrymple, R., Harris, L., and Liu, P. (editors), Coastal Engineering Manual, Part II , Coastal Hydrodynamics Chapter II-3 , Engineer Manual 1110-2-1100, U.S. Army Corps of Engineers, Washington, DC.

White, W. A., Tremblay, T. A., Wermund, E. G., Jr., and Handley, L. R. 1993. "Trends and status of wetlands and aquatic habitats in the Galveston Bay System, Texas," Galveston Bay National Estuary Prog. Pub. GBNEP No. 31, Webster, TX.

Yu, Y., Sternberg, R.W. and Beach, R.A. 1993. Kinematics of breaking waves and associated suspended sediment in the nearshore zone. Continental Shelf Research, 13, 1219-1242.

Zilkoski, D., Hall, L., Mitchell, G., Kammula, V., Singh, A. et al.. "The Harris-Galveston Coastal Subsidence District/National Geodetic Survey Automated Global Positioning System Subsidence Monitoring Project." 24 July 2006. http://www.subsidence.org/PDF_Files/GPSProject.pdf.

VITA

Name:	Robert C. Thomas
Address:	Texas A&M University Galveston, PO Box 1675, Galveston TX 77553
Email Address:	agamenon49@neo.tamu.edu
Education:	M.S., Ocean Engineering, Texas A&M University, 2007
	B.S., Maritime Systems Engineering, Texas A&M University Galveston, 2005